

2005

Metallo-dielectric photonic band gap structures fabricated using RF magnetron sputtering technology

Cijy Elizabeth Sunny
University of Dayton

Follow this and additional works at: https://ecommons.udayton.edu/graduate_theses

Recommended Citation

Sunny, Cijy Elizabeth, "Metallo-dielectric photonic band gap structures fabricated using RF magnetron sputtering technology" (2005). *Graduate Theses and Dissertations*. 5867.
https://ecommons.udayton.edu/graduate_theses/5867

This Thesis is brought to you for free and open access by the Theses and Dissertations at eCommons. It has been accepted for inclusion in Graduate Theses and Dissertations by an authorized administrator of eCommons. For more information, please contact mschlangen1@udayton.edu, ecommons@udayton.edu.

METALLO-DIELECTRIC PHOTONIC BAND GAP STRUCTURES FABRICATED
USING RF MAGNETRON SPUTTERING TECHNOLOGY

Thesis

Submitted to

The School of Engineering of the
UNIVERSITY OF DAYTON

in Partial Fulfillment of the Requirements for

The Degree

Master of Science in Electro-Optics

by

Cijy Elizabeth Sunny

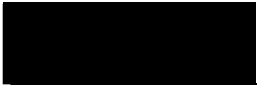
UNIVERSITY OF DAYTON

Dayton, Ohio


December, 2005

METALLO-DIELECTRIC PHOTONIC BAND GAP STRUCTURES FABRICATED
USING RF MAGNETRON SPUTTERING TECHNOLOGY


APPROVED BY:




Andrew M. Sarangan, Ph.D.
Assistant Professor,
Electro-Optics Program
University of Dayton
Committee Chairman




Joseph W. Haus, Ph.D.
Director and Professor,
Electro-Optics Program
University of Dayton
Committee Member



Qiwen Zhan, Ph.D.
Assistant Professor,
Electro-Optics Program
University of Dayton
Committee Member



Donald L. Moon, Ph.D.
Associate Dean
Graduate Engineering Programs & Research
School of Engineering



Joseph E. Saliba, Ph.D., P.E.
Dean, School of Engineering

CITY SUNNY

BOND PAPER
COPY 1

Heckman -

Please Do Not

Remove This Note

original

ABSTRACT

METALLO-DIELECTRIC PHOTONIC BAND GAP STRUCTURES FABRICATED USING RF MAGNETRON SPUTTERING TECHNOLOGY

Cijy Elizabeth Sunny
University of Dayton

Advisor: Dr. Andrew M. Sarangan

The technology of multi-layered thin films is essential for a variety of optical structures, such as optical filters, anti-reflection coatings and photonic band gap structures. These structures take advantage of combinations of materials with differing indices of refraction in a periodic (or quasi periodic) fashion to obtain novel transmission and reflection properties. The large index contrast between metals and dielectrics can be utilized to produce very broad reflection spectra (and correspondingly wide stop bands) using substantially fewer layers compared to all dielectric periodic structures. Furthermore, despite the high absorption coefficient of the metal films, a high transmission coefficient could be achieved by carefully placing the metal films at the field minima of the resonant wave.

In this thesis, an RF magnetron sputter deposition technique was developed for the fabrication of metallo-dielectric structures. Sputtering is a process where atoms are ejected out of a solid surface by highly energetic particles (plasma). In magnetron

plasma, a magnet behind the target causes the secondary electrons ejected from the target to travel in a spiral path, increasing the probability of further ionization of the sputtering gas. This results in high plasma densities and high deposition rates. Since the performance of metallo-dielectric structures is greatly influenced by the uniformity, surface roughness and stress of the thin films, careful calibration and characterization of the films is an essential step in the fabrication process. The film properties are affected by the chamber condition, base pressure, deposition pressure, RF power and target type. The process for determining these properties and the calibration values for each type of target material will be presented in this section.

The design of the metallo-dielectric structures was performed using a complex formulation of the transfer matrix method (TMM). The structure consists of four pairs of SiO_2 and Ag films, in different thicknesses for design verification. Simulations predict high transmission within the visible range, and strong attenuation outside this window. The device was fabricated in a dual-cathode sputtering chamber by alternating the shutter control of each target to allow high purity films to be consecutively deposited without exposing the intermediate layers to the ambient environment. The transmission characteristics of the structures were examined using a spectrophotometer and compared to the theoretical results for analysis and conclusions.

ACKNOWLEDGEMENTS

I would like to thank God for all His blessings. I would also like to thank my family for all their love and trust.

I would like to thank Dr. Andrew Sarangan, my advisor, for originating the idea for this research. He has guided me through this research process and provided me with the help I needed to complete this project. I would also like to thank Dr. Haus for providing the expertise regarding metallodielectric stacks and transparent metals. Dr. Zhan for helping me with the Atomic Force Microscope. NEST facility at the University of Dayton for their Scanning Electron Microscope and the Air Force base for the DC sputter tool for sputtering Nickel and their RTA (rapid thermal annealing) tool. Chemistry department at the University of Dayton for letting me use their UV visible spectrophotometer.

I would also like to thank all my Electro-Optics friends especially Kim and Aziz and the administrative staff, Trina, Nancy and Erin for all their valuable help.

TABLE OF CONTENTS

ABSTRACT.....	iii
ACKNOWLEDGEMENTS.....	v
LIST OF ILLUSTRATIONS.....	viii
LIST OF TABLES.....	xi
CHAPTER	
I. INTRODUCTION.....	1
II. SPUTTERING.....	4
Thin Film Deposition Techniques.....	4
Introduction to Sputtering.....	9
Physics of Sputtering.....	10
Deposition Rate: Sputter Yield.....	12
Sputtering Systems.....	12
Denton Vacuum Explorer®14 Sputtering System	16
Factors affecting Sputtered Thin Films.....	20
III THIN FILM CHARACTERIZATION.....	25
Calculation of Thickness Tooling Factor.....	25
Study of Argon Gas Pressure Vs Deposition Rate and Tooling	39
Thin Film Stress Measurement.....	42
Thin Film Roughness Measurement.....	48
IV METALLO-DIELECTRIC STACKS.....	53
Transfer Matrix Method.....	56
Dispersion profile for Ag and SiO ₂	60
MD stack-1.....	61
MD stack-2.....	64
MD stack-2A.....	67
MD stack-3.....	68
MD stack-1A	70

	Roughness Measurements for the Stacks.....	73
V	CONCLUSIONS.....	76
	Conclusions.....	76
	Summary of Contributions.....	77
	Future Research.....	78
	REFERENCES.....	80
	VITA.....	83

LIST OF ILLUSTRATIONS

1. Figure 2.1.....	4
2. Figure 2.2.....	5
3. Figure 2.3.....	6
4. Figure 2.4.....	7
5. Figure 2.5.....	10
6. Figure 2.6.....	11
7. Figure 2.7.....	13
8. Figure 2.8.....	14
9. Figure 2.9.....	14
10. Figure 2.10.....	16
11. Figure 2.11.....	16
12. Figure 2.12.....	17
13. Figure 2.13.....	18
14. Figure 2.14.....	19
15. Figure 2.15.....	20
16. Figure 2.16.....	21
17. Figure 2.17.....	22
18. Figure 2.18.....	24
19. Figure 3.1.....	27

20. Figure 3.2.....	27
21. Figure 3.3.....	28
22. Figure 3.4.....	29
23. Figure 3.5.....	30
24. Figure 3.6.....	31
25. Figure 3.7.....	33
26. Figure 3.8.....	34
27. Figure 3.9.....	35
28. Figure 3.10.....	36
29. Figure 3.11.....	37
30. Figure 3.12.....	38
31. Figure 3.13.....	39
32. Figure 3.14.....	40
33. Figure 3.15.....	41
34. Figure 3.16.....	43
35. Figure 3.17.....	49
36. Figure 3.18.....	50
37. Figure 3.19.....	51
38. Figure 4.1.....	54
39. Figure 4.2.....	55
40. Figure 4.3.....	57
41. Figure 4.4.....	60
42. Figure 4.5.....	61

43. Figure 4.6.....	62
44. Figure 4.7.....	63
45. Figure 4.8.....	65
46. Figure 4.9.....	66
47. Figure 4.10.....	67
48. Figure 4.11.....	68
49. Figure 4.12.....	69
50. Figure 4.13.....	70
51. Figure 4.14.....	71
52. Figure 4.15.....	72
53. Figure 4.16.....	74
54. Figure 4.17.....	74
55. Figure 4.18.....	75

LIST OF TABLES

1. Table 3.1.....	26
2. Table 3.2.....	45
3. Table 3.3.....	45
4. Table 3.4.....	47
5. Table 3.5.....	47

CHAPTER I

INTRODUCTION

This thesis describes the application of RF magnetron sputtering to fabricate thin films for advanced optoelectronic applications. The work was performed on a newly acquired Denton Vacuum Explorer®14 thin film deposition system. This was the first use of this tool at the University of Dayton; hence the work described here includes basic performance verifications and thin film calibrations in addition to the design, fabrication and measurement of the multi-layer structures. The structures fabricated for this work all involve metals and dielectrics, and are generally referred to as metallo-dielectric stacks.

The technology of multi-layered thin films is essential for a variety of optical structures, such as optical filters, anti-reflection coatings and photonic band gap structures. These structures take advantage of combinations of materials with differing indices of refraction in a periodic fashion to obtain novel transmission and reflection properties. The large index contrast between metals and dielectrics can be utilized to produce very broad reflection spectra, and correspondingly wide stop bands, using substantially fewer layers compared to all-dielectric periodic structures. Furthermore, despite the high absorption coefficient of the metal films, a high transmission coefficient could be achieved by carefully placing the metal films at the field minima of the resonant wave.

The thesis is organized as follows:

A basic overview of sputtering technology and the factors that influence the thin films are described in Chapter II. This chapter also includes a brief description of the Denton Vacuum Explorer®14 tool and its capabilities. Sputtering is a process where atoms are ejected out of a solid surface by highly energetic particles (plasma). In a magnetron plasma, a magnet behind the target causes the secondary electrons ejected from the target to travel in a spiral path, increasing the probability of further ionization of the sputtering gas. This results in high plasma densities and high deposition rates. Since the performance of metallo-dielectric structures is greatly influenced by the uniformity, surface roughness and stress of the thin films, careful calibration and characterization of the films is an essential step in the fabrication process. The film properties are affected by the chamber condition, base pressure, deposition pressure, RF power and target type. The process for determining these properties and the calibration values for each type of target material will be presented. The characterization of the thin films and how the film properties depend on the deposition conditions is described in Chapter III.

In Chapter IV, the design, fabrication and measurement of the metallo-dielectric stacks is described. The design was performed using a complex formulation of the transfer matrix method (TMM) using the LIGHTS software. The structure consists of four pairs of SiO₂ and Ag films, in different thicknesses for design verification. Simulations predict high transmission within the visible range, and strong attenuation outside this window. Since the Explorer 14 features a dual-cathode vacuum chamber, the metallo-dielectric stacks were made by alternating the shutter control of each target. This allowed for high purity

films to be consecutively deposited without exposing the intermediate layers to the ambient environment. The transmission characteristics of the structures were examined using a spectrophotometer and compared to the theoretical results for analysis and conclusions. Also a study of the roughness measurements for each these different designs that were fabricated are also presented in this chapter.

CHAPTER II

SPUTTERING

Thin Film Deposition Techniques¹³

Thin solid films are fabricated by the deposition of individual atoms on a substrate. Their thicknesses are typically only a few hundred Angstroms. They are widely used for making electronic devices, optical coatings and decorative parts. They are necessary for the development of novel optical devices, Bragg stacks (spectrally tuned reflector), AR (anti reflection) coatings, wear resistant films, etc., to name a few. Typical deposition methods of thin films are shown in figure 2.1.

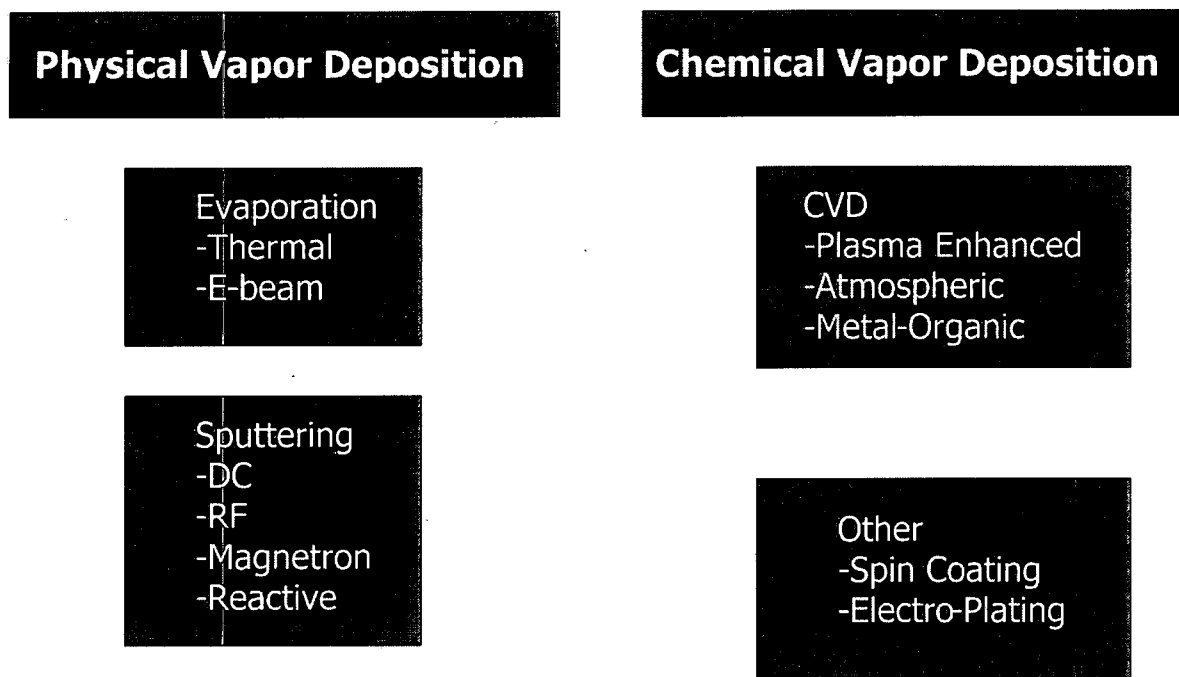


Figure 2.1 Thin film Technologies

The deposition methods are composed of the physical vapor deposition (PVD) process and the chemical vapor deposition (CVD) process.

Physical Vapor Deposition:

Thermal Evaporation: This process comprises evaporating source materials in a vacuum chamber below 1×10^{-6} Torr and condensing the evaporated particles on a substrate. In

Resistance heated evaporation, an electric resistance heater is used to melt the material and raise its vapor pressure to a useful range as shown in the figure 2.2. This is done in a high vacuum, both to allow the vapor to reach the substrate without reacting with or scattering against other gas-phase atoms in the chamber, and to reduce the incorporation of impurities from the residual gas in the vacuum chamber. The disadvantage of this method is that only materials with a much higher vapor pressure than the heating element can be deposited without contamination of the film. As a result high purity films are hard to obtain.

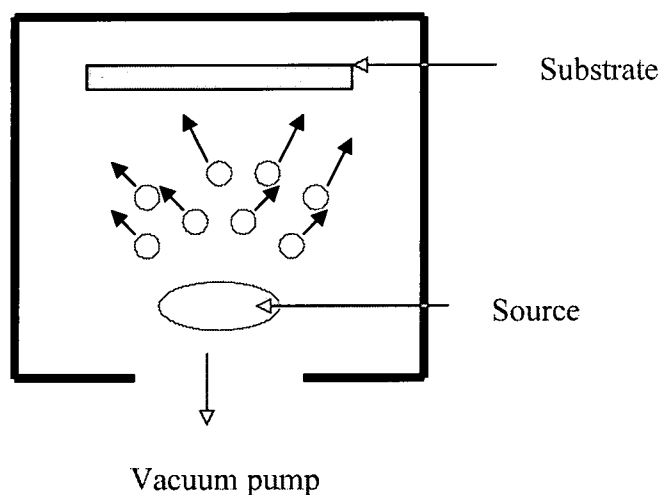


Figure 2.2 Resistance heated evaporation¹⁸

Electron beam evaporator fires a high-energy beam from an electron gun to boil a small spot of material as shown in the figure 2.3. Since the heating is not uniform, lower vapor pressure materials can be deposited. Through a high acceleration voltage the electrons come out of the gun and the beam being highly focused, hits the target material only. As a result this leads to high purity films and better control of deposition rates. This is suitable for high melting temperature (3000°C) metals like platinum. It's a slower and more expensive compared to resistance heated evaporation.

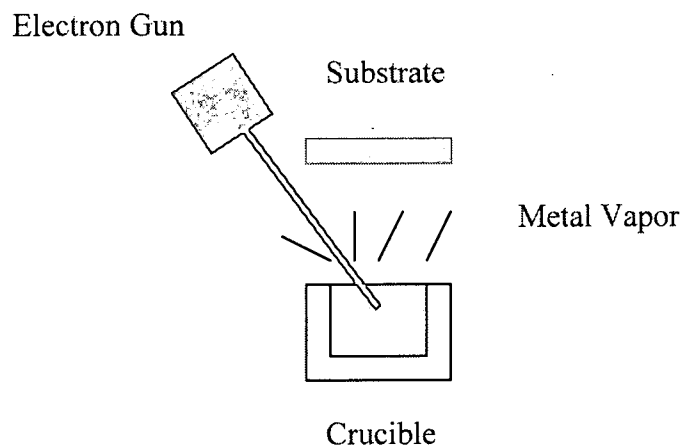


Figure 2.3 Electron-beam evaporation¹⁸

Sputtering: When a solid surface is bombarded with energetic particles such as accelerated ions, surface atoms of the solid are scattered backward due to collisions between the surface atoms and the energetic particles as shown in figure 2.4. This phenomenon is called sputtering. This will be discussed in detail in the next section.

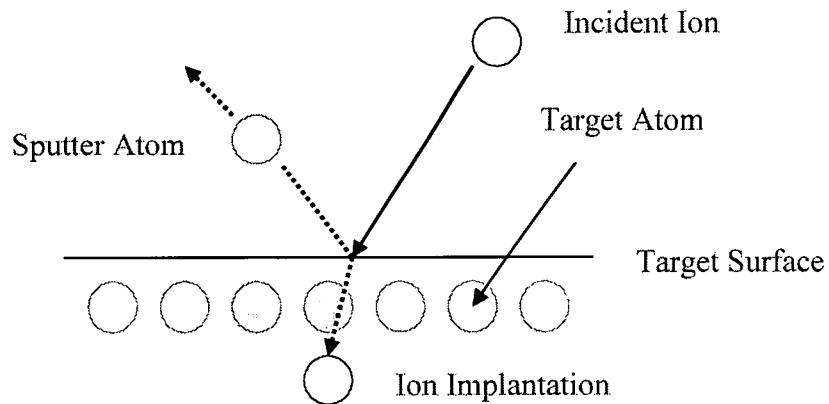


Figure 2.4 Physical sputtering processes¹³

Sputtering has a better step coverage than evaporation, induces far less radiation damage than electron beam evaporation, and is much better at producing layers of compound materials and alloys. Sputtering also called spluttering and cathode disintegration, is the metal deposition technique of choice for most silicon based technologies.

Chemical Vapor Deposition:

CVD is a widely used method for depositing thin films by chemical reaction. Applications of CVD range from the fabrication of microelectronic devices to the deposition of protective coatings. In a typical CVD process, reactant gases (often diluted in a carrier gas) are introduced into the chamber and heated radiatively. Depending on the process and operating conditions, any solid byproducts of the chemical reaction will precipitate on the substrate to form the thin film.

Plasma enhanced chemical vapor deposition (PECVD) is an important deposition method for the fabrication of VLSI (very large-scale integration) circuits and TFTs (thin film transistors). Its main advantage compared to the conventional CVD method is that it is a low temperature process. In this technique the reactant gases are introduced into the chamber and ionized into a plasma by an RF source to promote the reaction. The byproducts of the reaction will precipitate on the substrate to form the film. Since a plasma is used to accelerate the reaction instead of radiative heating, this is suitable for temperature sensitive substrates such as polymers or metals with a low-melting point.

Atmospheric pressure chemical vapor deposition (APCVD) is performed in a reactor at temperatures up to $\sim 400^{\circ}\text{C}$. The deposited film is a product of a chemical reaction between the source gases supplied to the reactor. This CVD process is done at atmospheric pressure and it yields high reaction rates of $1000\text{\AA}/\text{min}$. It has a poor step coverage and particle contamination.

Metal Organic Chemical Vapor Deposition (MOCVD) or Metal-Organic Vapor Phase Epitaxy (MOVPE) is a widely used method for preparing epitaxial structures by depositing atoms on a crystalline substrate and is typically used to grow compound semiconductors. Atoms are deposited by decomposing organic molecules by passing over the hot substrate. It has accurate control of composition, doping and thickness of the films deposited. It has a faster growth rate of $3\mu\text{m}/\text{hr}$.

Spin Coating²⁶ and Electroplating Spin coating is the preferred method for application of thin, uniform films to flat substrates. An excess amount of polymer solution is placed on the substrate using a nozzle that pours the coating solution out, or it could be sprayed

onto the surface. The substrate is then rotated at high speed in order to spread the fluid by centrifugal force. Rotation is continued for sometime, with fluid being spun off the edges of the substrate, until the desired film thickness is achieved. The solvent is usually volatile, providing for its simultaneous evaporation.

Electroplating is achieved by passing an electrical current through a solution containing dissolved metal ions and the metal object to be plated. The metal object serves as the cathode in an electrochemical cell, attracting metal ions from the solution. Ferrous and non-ferrous metal objects are plated with a variety of metals, including aluminum, brass, bronze, cadmium, copper, chromium, iron, lead, nickel, tin, and zinc, as well as precious metals, such as gold, platinum, and silver. The process is regulated by controlling a variety of parameters, including the voltage and current, temperature, and the purity of bath solutions.

Introduction to Sputtering

The verb to SPUTTER originates from Latin SPUTARE (to emit saliva with noise). This phenomenon was first described 150 years ago. Sputtering is the primary alternative to evaporation for metal film deposition in microelectronics fabrication. First discovered in 1852, by W.R.Grove, sputtering was developed as a thin film deposition technique by Langmuir in the 1920s.

The simplest configuration of a sputtering system is a parallel plate arrangement held in a vacuum chamber as shown in fig 2.5. In many respects it is very similar to a parallel plate

reactive ion etch system. In a sputtering application, the plasma chamber must be arranged so that a high density of ions strikes the target containing the material to be deposited. Hence, the target material must be placed on the electrode with the maximum ion flux. In contrast, in a reactive ion etch application the sample is held at the electrode with the highest ion flux. To collect most of the ejected atoms from the sputtered target, the cathode and anode in a typical sputtering system are closely spaced, often less than 10cm. An inert gas, typically Ar, is normally used as the backfill gas to prevent chemical reaction between the sputtered species and the ions. In some cases, reactive gases could be combined with the inert backfill to produce sputtered species that are chemically different from the target material. The gas pressure in the chamber is held at about 100mT during deposition.

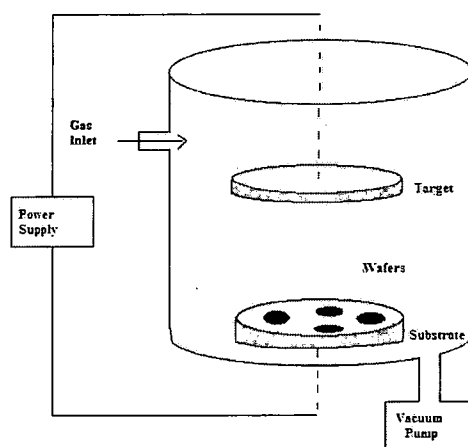


Figure 2.5 Chamber for a simple parallel plate sputtering system¹²

Physics of Sputtering

When an energetic ion strikes the surface of a material, four physical processes can happen as shown in the figure 2.6. Ions with very low energies will simply bounce off the

surface. At energies of about 10 eV, the ion may also adsorb to the surface, giving up its energy to phonons (heat). At energies above about 10 KeV, the ion penetrates many atomic layers into the material, depositing most of its energy deeper into the substrate. These high energies are typical for ion implantation applications.

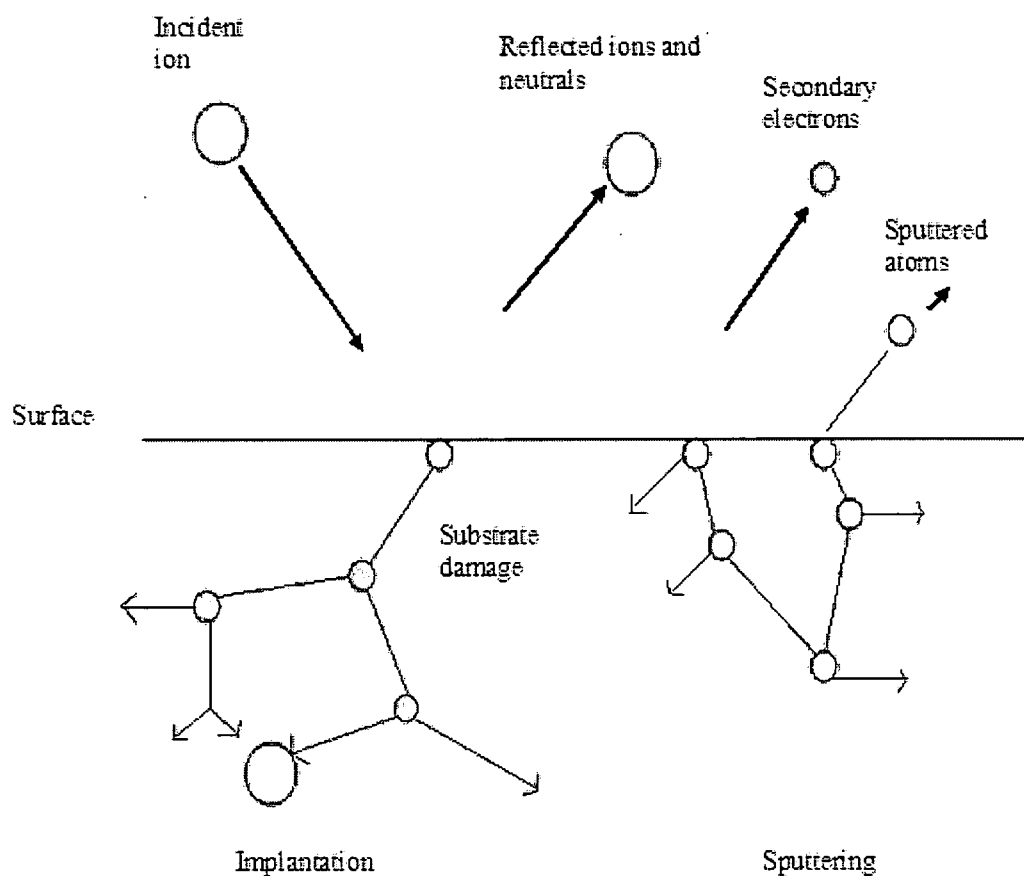


Figure 2.6 Possible outcomes for an ion incident on the surface of a wafer¹²

At high energies like those used in implantation, chemical bonding of the target atoms can be largely ignored and the target can be considered simply a collection of atoms. At very low energies, no disruption of the target occurs. An ion incident on the target surface may travel several atomic layers into the target until it strikes an atom nearly head on and

is deflected through a large scale. This near head on collision may also liberate a target atom that has a large momentum directed at a significant angle with respect to the surface normal. During this process many of the bonds in the top layers of the target will be broken. If several of these large angle collisions occur, the incident atom or the recoiled atom may develop a significant velocity component parallel to the surface of the wafer. A subsequent collision can then eject an atom or small cluster of atoms.

Deposition Rate: Sputter Yield^{12, 13}

The sputter deposition rate depends on the ion flux to the target, the probability that the impact of an incident ion will eject a target atom and the transport of the sputtered material across the plasma to the substrate. The sputter yield S , which is the removal rate of surface atoms due to ion bombardment, is defined as the mean number of atoms removed from the surface for each incident ion and is given by,

$$S = \text{atoms removed/incident atoms}$$

Sputtering systems^{12, 17}

DC sputtering: The DC diode sputtering system is composed of a pair of planar electrodes. One of the electrodes is a cold cathode and the other is an anode. The plasma-facing surface of the cathode is covered with a target material and the reverse side is water-cooled. The substrates are placed on the anode. When the sputtering chamber is kept in argon gas at around 100mT with several kilovolts of dc voltage applied to the electrodes, the glow discharge is initiated. The Ar ions in the glow discharge are accelerated at the cathode and sputter the target, resulting in the deposition of a thin film on the substrates. In the DC diode system, sputtered particles collide with gas molecules

and then eventually diffuse to the substrate since the gas pressure is so high and the mean free path of the sputtered particles is less than the electrode spacing. By simple substitution of an insulator target for the metal target in a DC diode sputtering system, the sputtering glow discharge can not be sustained because of the immediate build-up of a surface charge of positive ions on the front side of the insulator. As a result this can be use only for metals and not dielectrics. Figure 2.7 shows a DC diode sputtering system.

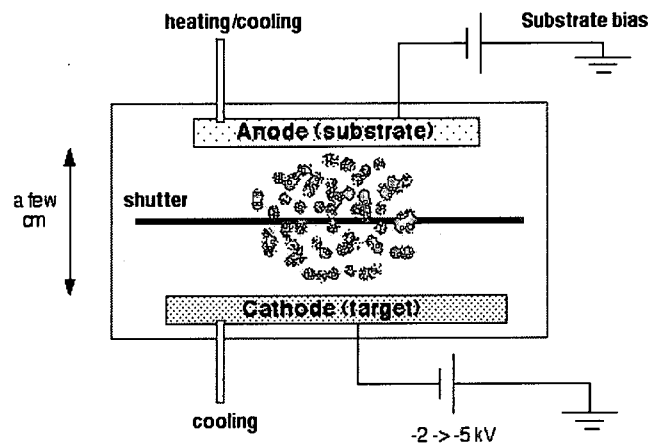


Figure 2.7 DC diode sputtering¹⁷

RF (Radio Frequency) Sputtering: In order to sustain the glow discharge with an insulator target, the DC voltage power supply is replaced by an RF power supply. This RF sputtering system is used for the deposition of dielectric materials. The RF diode sputtering system requires an impedance-matching network between the power supply and the discharge chamber. In the RF discharge system the operating pressure is lowered to as low as 1mTorr, since the RF electric field in the discharge chamber increases the collision probability between secondary electrons and gas molecules.

Figure 2.8 shows a RF sputtering system. The target area is much smaller than the grounded anode and the chamber wall. This asymmetric electrode configuration induces a DC bias on the target, and this causes sputtering in the RF system. Sputtering occurs when the target is negatively biased as shown in the figure 2.9

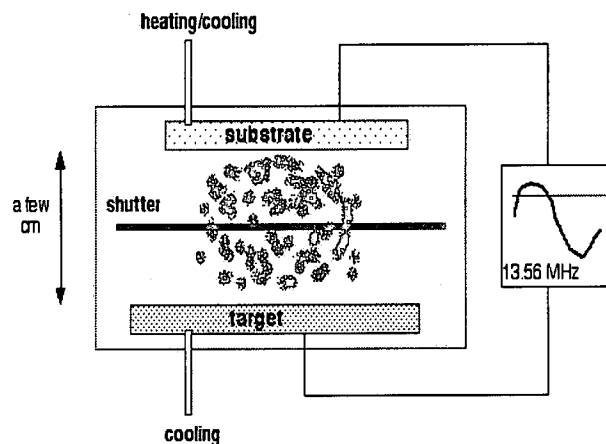


Figure 2.8 RF sputtering system¹⁷

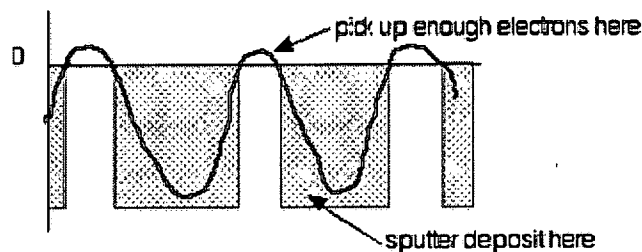


Figure 2.9 RF sputtering¹⁷

Magnetron Sputtering: This can be used with a RF or DC source. It increases the ionization of Ar and thus increases the sputter rates at lower Ar pressures (down to 0.5 mTorr). The application of a magnetic field in the plasma causes the electrons to spiral

around the direction of the magnetic field lines. The radius of this orbital motion is given by

$$r = \frac{mv}{q} B$$

The orbital motion of the electrons increases the probability that they will collide with neutral species and create ions. The use of a magnetron also allows the formation of plasma at lower chamber pressures, typically around 1-5mTorr.

Figure 2.10 shows two geometries that have been used for magnetron sputtering. A planar magnetron starts with the basic parallel plate reactor as shown in the Figure 2.5. The Denton vacuum Explorer®14 system uses a 3.0" diameter, Angstrom Science planar magnetron sputter sources. Either a solenoid coil or a set of magnets is added behind the target in such a way as to create magnetic field lines parallel to the surface of the target. Circular planar magnetron targets can be made by arranging the bar magnets radially from the center of the target. A cylindrical magnetron starts with a cylindrical plasma chamber with a target electrode at the center. The wafer holding electrode is the vertical wall of the chamber. The magnetron is added by inserting the chamber in an electromagnetic winding that generates a vertical field. Figure 2.11 shows a crossed electric and magnetic field. This type of system is of less interest to microelectronic production due to the difficulty with placing large diameter wafers on the walls of a cylindrical chamber. A typical field for either type of system is a few hundred Gauss.

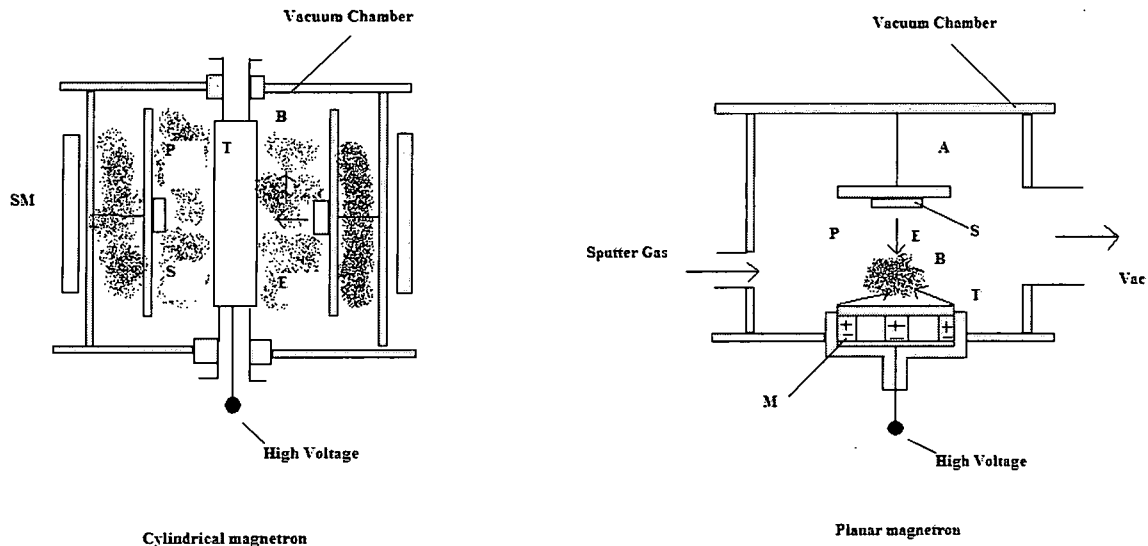


Figure 2.10 Planar and cylindrical magnetron sputtering systems T: target; P: plasma; SM: solenoid; M: magnet; E: electric field; B: magnetic field¹²

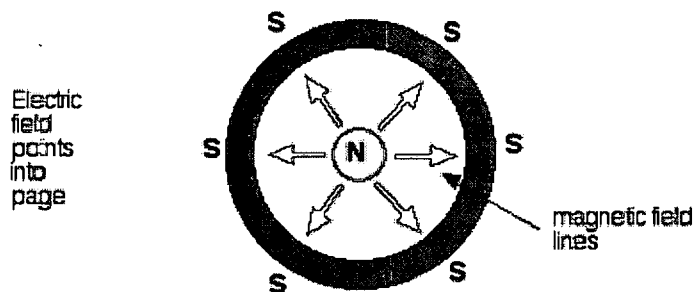


Figure 2.11 Crossed electric and magnetic fields¹⁷

Denton Vacuum Explorer®14 Sputtering System²⁴

Introduction: The Denton Vacuum Explorer®14 Coating System is a vacuum deposition system designed for precision thin film applications. This system is semi-automatic and is controlled by a CPU. The operator interface is a touch panel with graphical interface to the PLC as shown in the figure 2.12. Manual operation of valves, pumps, power sources,

and fixture rotation subsystems is through this graphical interface. Automatic processes are also operated through this interface. The touch panel, gauges, switches, deposition controller, and subsystem controllers are installed in one electrical control cabinet.

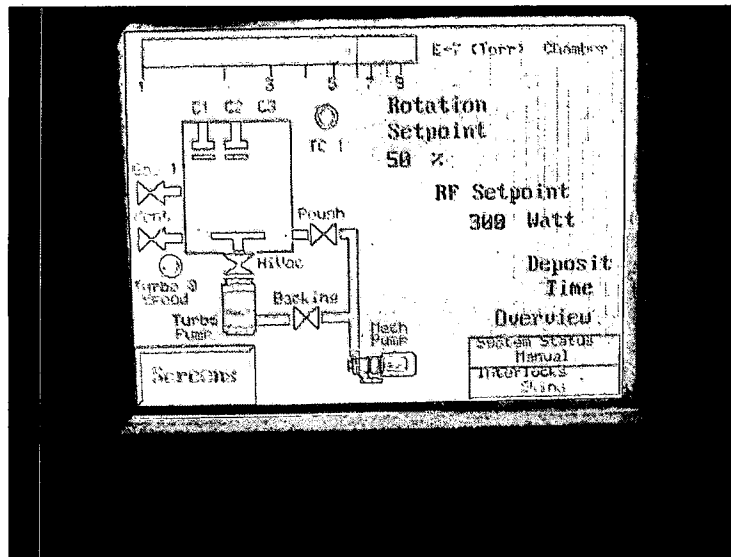


Figure 2.12 Overview screen

Deposition Chamber: The Denton Vacuum Explorer@14 system has a stainless steel chamber with a 12"×13" front loading door. The door has an optically shielded 4.0" diameter view port to permit viewing of the target plasma and substrate fixturing. O-rings and seals are used for all ports to maintain a high vacuum in the chamber. Figure 2.13 shows the sputtering system.

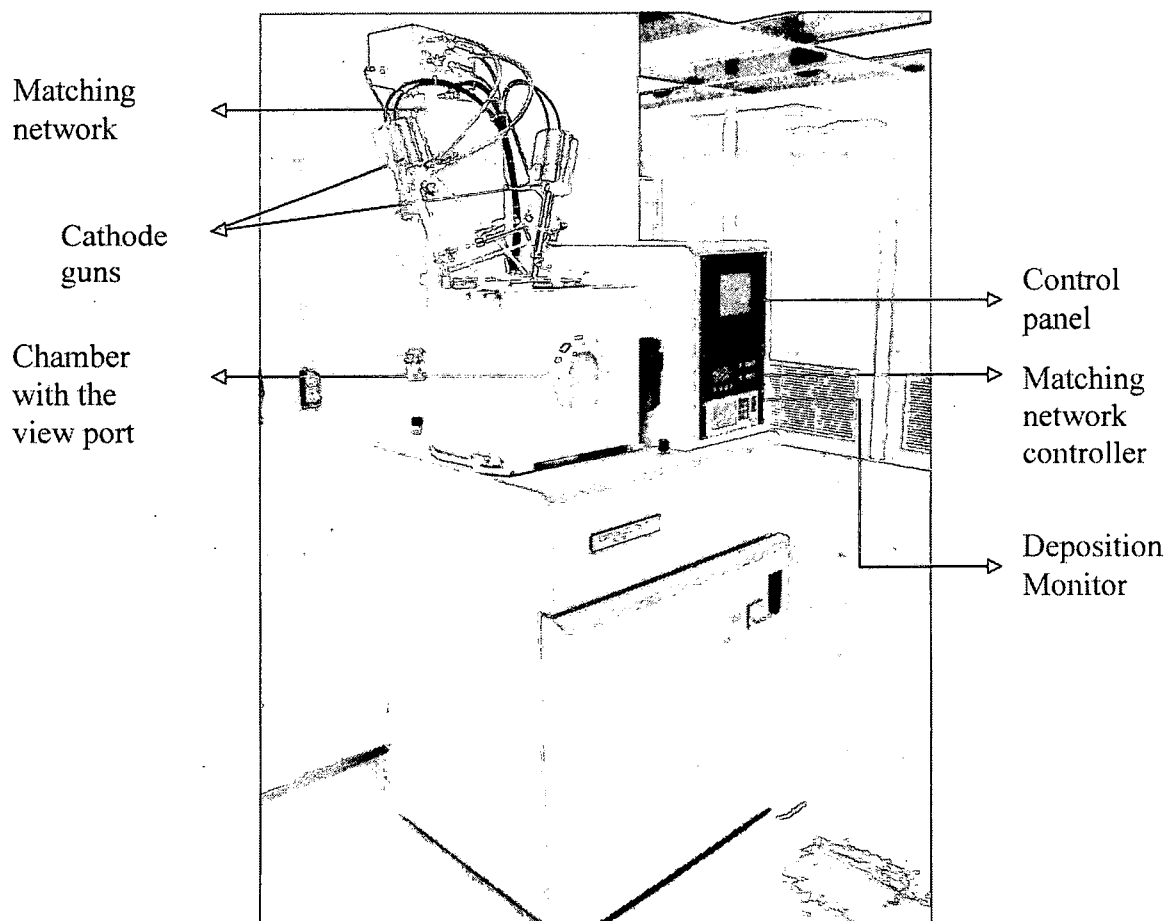


Figure 2.13 Denton Vacuum Explorer®14 sputtering system

Deposition System: This tool uses a Pfeiffer turbo-molecular pump that can reach vacuum levels as low as 10^{-8} Torr. An Inficon crystal monitor controls the film thickness during deposition. The 4" substrate can be rotated during deposition for uniform coverage. This equipment uses 3.0" diameter, Angstrom Science planar magnetron sputter sources. Each source has a shutter which is interfaced to system PLC for remote open/close operation. It uses 600W RF power supply with matching network. The impedance matching network is used to match the impedances of the plasma and the RF.

It also has a 4.0" rotating substrate fixture plate for an even film deposition with a chain drive and the speed of rotation of this substrate can be adjusted via the input to system touch screen. Figure 2.14 shows the interior view of the deposition chamber.

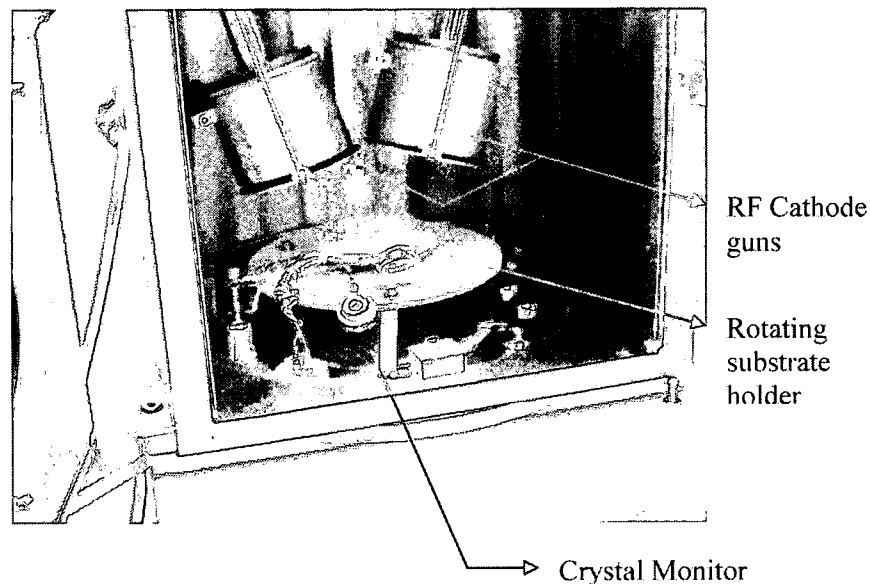


Figure 2.14 Inside view of the deposition chamber

Inficon Deposition Monitor-Calibration and Measurement: A quartz crystal is used for real-time monitoring of the film thickness during deposition. The quartz crystal microbalance is capable of precisely measuring the mass added to the face of the oscillating quartz crystal sensor. The instrument's knowledge of the density of this added material (specified by the film's density parameter) allows conversion of the mass information into thickness. Because the crystal is not at the same location as the substrate as shown in the figure 2.15, it is necessary to account for the different amount of material

on the sensor compared to the substrate. This factor is accounted for by a tooling parameter, which can be programmed into the crystal monitor software.



Figure 2.15 Sputtering of Ag

Factors affecting Sputtered Thin films

The properties of sputtered thin films depend upon various factors:

Tooling Factor: This is a calibration factor that adjusts for the difference in film thickness between the substrate and the crystal monitor. This differs for every target material and deposition condition. Hence the deposition monitor needs to be calibrated for different materials. Detailed studies of this tooling factor for the various materials are discussed in chapter III. The term “tooling factor” is widely used in the industry to represent this calibration factor.

Thermal Conductivity of the Target: The thermal conductivity of the target plays an important role in sputtering because it can affect the temperature of the target during deposition. Insulating targets will have poor thermal bonding with the cooling plate, and can reach very high temperatures and develop “hot spots”. Furthermore, large temperature cycling of the target can create cracks and defects and eventual disintegration of the target as shown in the figure 2.16. Hence dielectric targets are typically more difficult to sputter than metals. One approach is to coat the dielectric targets with Ag or Indium target paste as shown in figure 2.17 to improve the bonding between the target and the copper backing plate. This requires constant monitoring because over time, this paste may dry and lose its thermal conductivity, or may not evenly spread on the target before placing it in the target holder.

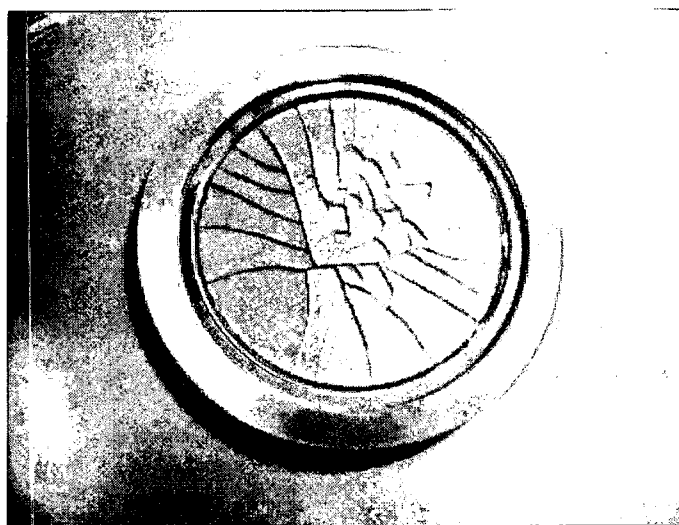


Figure 2.16 An example of a cracked target¹⁹



Figure 2.17 Target coated with Ag target paste

Process Gas Pressure: The deposition rate and flux distribution of the target species are significantly affected by the process gas pressure. Typically, the deposition rate exhibits a maximum as function of pressure, which is considered to be the optimum deposition condition. However, since the flux distribution also changes with pressure, we can expect the tooling factor to also become a strong function of process gas pressure. This is described in the chapter on thin film characterization, chapter III. In addition, step coverage of the thin film is also significantly affected by gas pressure. As the gas pressure decreases, the target species become more directional due to fewer collisions with the Ar atoms. As a result, the deposition becomes more anisotropic resulting in poor step coverage. At higher gas pressures, the target species undergo many collisions with the Ar atoms resulting in a more isotropic deposition and better step coverage.

Chamber Condition: Since the Denton Vacuum Explorer®14 has no load lock attachment to the main chamber, the entire chamber is vented and exposed to the atmosphere before and after every deposition i.e., the chamber is exposed to atmospheric pressure when the samples are taken out or loaded into the chamber. For high purity thin films, a clean chamber devoid of any contaminants is important. Contamination can occur in the form of particulates in the atmosphere, or from outgassing thin films deposited on the chamber walls during prior depositions. Outgassing refers to sources of gas “stored up” inside the vacuum chamber and released slowly into the vacuum. To prevent outgassing, the chamber is covered with Aluminum foil and changed on a regular basis. We observed that when the chamber is open for a long time, for example when the targets are changed or sample loading or unloading, it takes more than 35 minutes to reach a base pressure of $10\mu\text{Torr}$ from 150mTorr turbo cross-over pressure. When the chamber has been closed and held under high vacuum for a long time, it is able to reach the same base pressure in a few seconds. Hence, moisture dramatically affects the pumping rate of the chamber. If moisture is not completely removed, it will react with the sputtered material and cause oxidation.

If the Aluminum foil is not changed periodically, the old films can outgas and react with the new films. For example, when sputtering metals like Ag after previous depositions of SiO_2 , the chamber will turn black as shown in the figure 2.18. This is due to the oxidation of the Ag from the oxygen outgas from the old SiO_2 films on the chamber walls. One technique to avoid this after sputtering SiO_2 is to purge the chamber with the Ar process gas for several minutes, to eliminate as many O_2 molecules as possible from the chamber

walls. But it was observed later that this purging with Ar for 10min did not make any difference and this is further explained in the chapter on metallo dielectric stacks, chapter IV.



—————> Deposition on the chamber

2.18 Chamber after Deposition of silver and SiO_2

CHAPTER III

THIN FILM CHARACTERIZATION

Calculation of Thickness Tooling Factor

Since the quartz sensor is displaced about 4 inches from the center of the sample stage, the thickness recorded by the sensor will typically be quite different from the sample. A Tooling Factor is used to adjust for this difference. Since the deposition flux distribution will vary with target material and deposition conditions, a separate tooling factor must be determined for each deposition scenario. Using an initial estimated tooling factor we make a short deposition on a test sample and determine the actual thickness with stylus profilometer. The correct tooling factor is calculated from the relationship,

$$Tooling(\%) = TF_i \left(\frac{T_m}{T_x} \right)$$

where T_m is the measured thickness; T_x is the thickness reading on the crystal monitor, TF_i is the initial estimated tooling factor.

Because of several parameters that affected the thin films as mentioned in Chapter II, it was observed that every time a deposition was made, the measured thickness of the film varied and so did the tooling factor. In order to verify the tooling factor before and after the metallo dielectric stacks were fabricated, a pre and post stack tooling measurements were carried out and the results are as discussed in the following sections. This new measured tooling factor was used to fabricate the next stack. For this study a total of five stacks were fabricated namely MD stack1, stack2, stack2A, stack3 and stack1A. An 'A'

suffixed to the stack names indicate that they were a replica of their original designs.

Table 3.1 shows a difference in each of the stacks based on the sputter parameters.

Table 3.1 Summary of 5 different stacks that were fabricated based on the sputter parameters

STACK NAME	Ar GAS PRESSURE(mTorr)		NO: OF LAYERS	FILM THICKNESS (Å)	
	Ag	SiO ₂		Ag	SiO ₂
1	2	2	9	170	2576
2	2	1.5	8	80	2000
2A	5	5	8	80	2000
3	5	5	9	50	2000
1A	2	2	8	170	2300

Pre MD stack 2 tooling factor:

Silver (Ag): 2000Å of Silver was deposited on a plain glass substrate at a Ar gas pressure of 2mTorr. Small holes were made on the thin film by marking the glass substrate with a sharpie marker pen prior to the deposition, and then using acetone liftoff techniques in an ultrasonic bath. An example of a silver coated sample with holes is shown in figure 3.1. The holes were then used to measure the step height of the thin film using the stylus profilometer, as shown in figure 3.2. The scan was performed across every hole and an average was taken as the final thickness. Figure 3.3 shows a typical distribution of thicknesses across a sample.

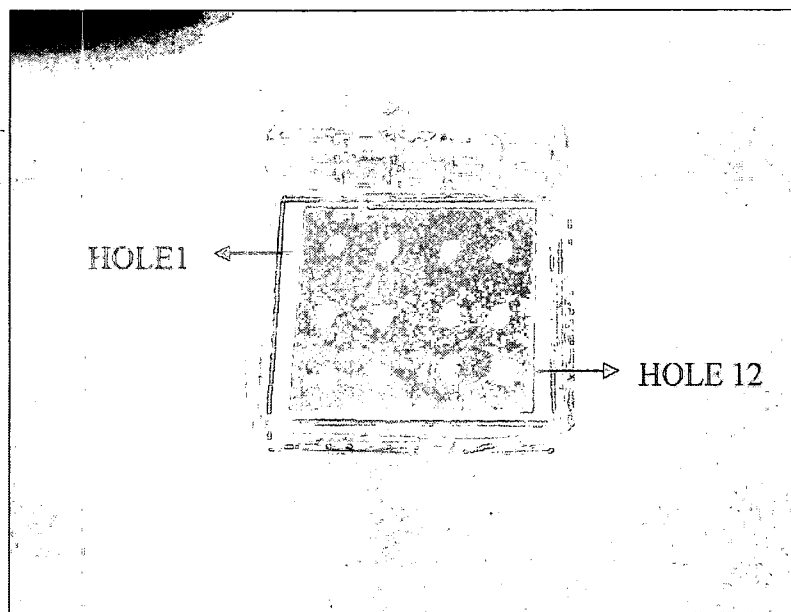


Figure 3.1 Holes created on a silver thin film using the lift-off technique

The tilt in Figure 3.2 is most likely caused by the film stress on the substrate.

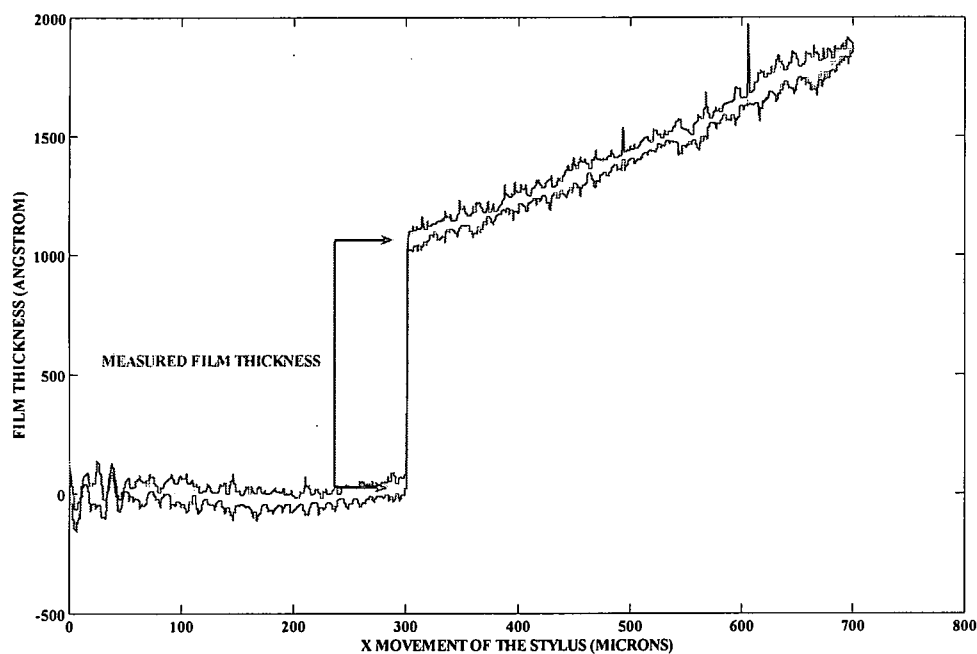


Figure 3.2 Profiler scan for a 1000Å Ag film

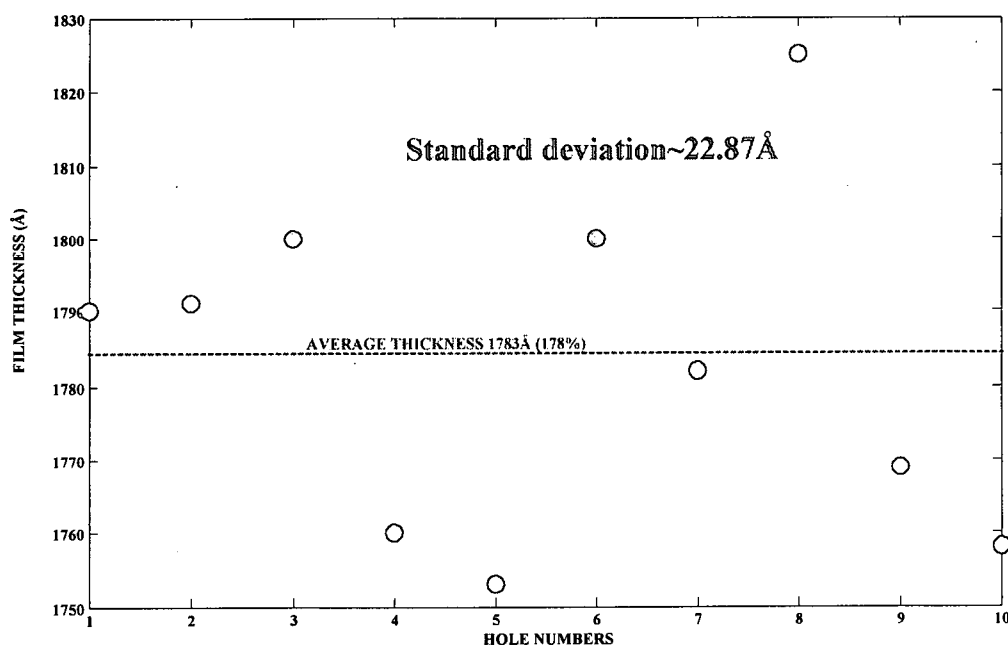


Figure 3.3 Thickness measurements across the different holes on the 2000Å Ag sample

T_m = Measured thickness (average over 10 scans) as measured by the profiler = 1783Å

T_x = Thickness reading on the Inficon deposition display = 2000Å

TF_i = Initial estimated tooling factor = 200%

Tooling factor (%) = $200 * (1783/2000) \sim 178\%$

Silicon dioxide (SiO₂): Figure 3.4 shows the thickness measurement across each hole of a 2000Å SiO₂ film sputtered at 1.5 mTorr of Ar gas pressure.

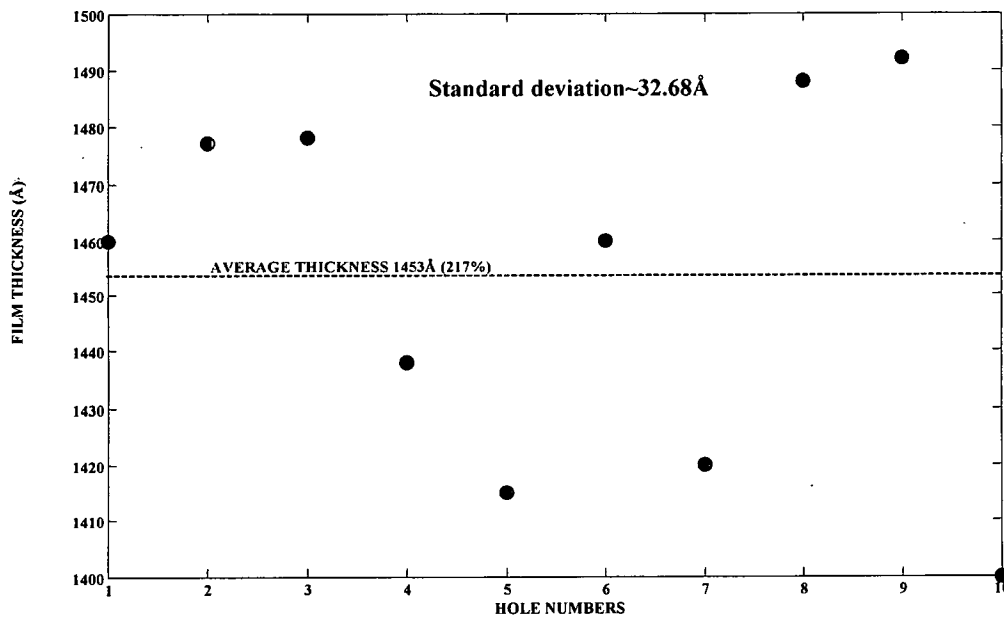


Figure 3.4 Thickness measurements across the different holes on the SiO₂ 2000Å sample

$$T_m = 1453\text{Å}$$

$$T_x = 2009\text{Å}$$

$$TF_i = 300\% \text{ (tooling factor for } 2009 \text{ Å)}$$

$$\text{Tooling factor (\%)} = 300 * (1453/2009) \sim 217\%$$

Post MD stack 2 tooling measurement:

After fabricating MD stack 2, another tooling was done on the Ag and SiO₂ layers and the thickness measurements are as shown in figure 3.5 and 3.6 respectively. The sputter parameters (gas pressure and RF power) were the same as in the earlier pre MD stack2 case. The initial estimated tooling factor was the one that was found prior to the fabrication of the stack.

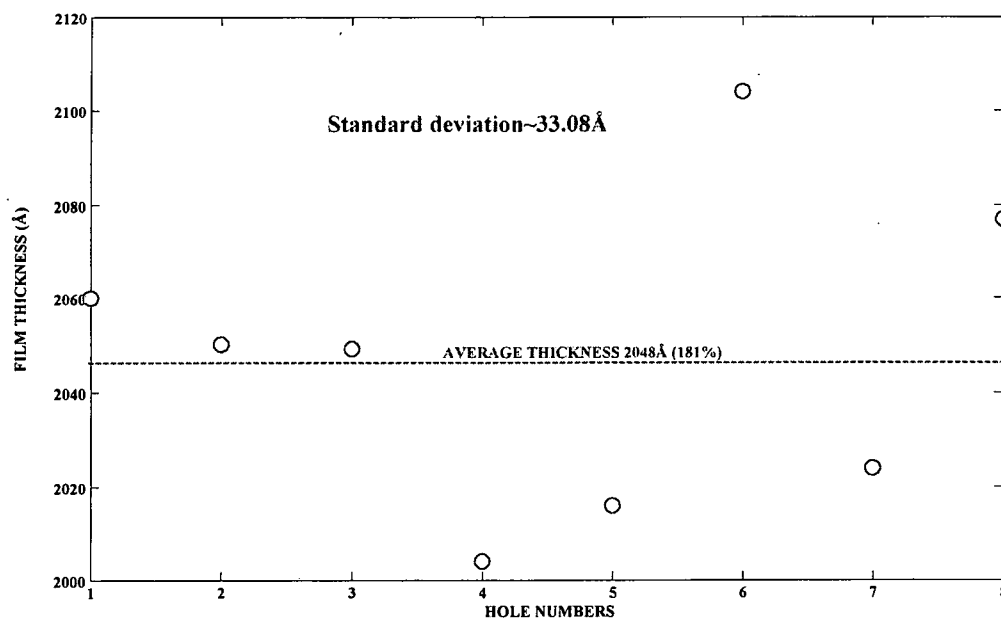


Figure 3.5 Thickness measurements across the different holes on the Ag 2000Å sample

$$T_m = 2048\text{Å}$$

$$T_x = 2010\text{Å}$$

$$TF_i = 178\% \text{ (tooling factor for } 2010\text{Å)}$$

$$\text{Tooling factor (\%)} = 178 * (2048/2010) \sim 181\%$$

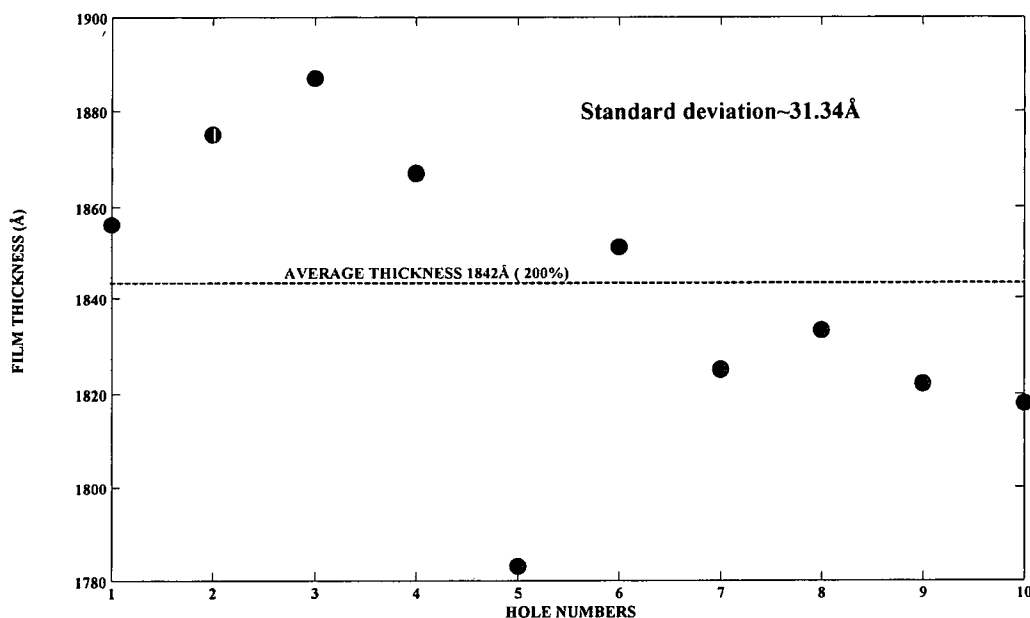


Figure 3.6 Thickness measurements across the different holes on the SiO₂ 2000Å sample

$$T_m = 1842\text{Å}$$

$$T_x = 2002\text{Å}$$

$$TF_i = 217\% \text{ (tooling factor for } 2002\text{Å)}$$

$$\text{Tooling factor (\%)} = 217 * (1842/2002) \sim 200\%$$

The tooling factor for Ag did not change much but the tooling factor for SiO₂ decreased. The reason for the tooling factor for SiO₂ causing a problem could be because the crystal monitor was also made of quartz and so it was not able to measure the very thick layers of SiO₂. The only parameter that changed was the crystal life (the ability of the crystal to measure the deposited thickness which is expressed in terms of a percentage). For the earlier sputtering the crystal life was 1% and for this study it was 3%. Crystal life is displayed as a percentage of the monitor crystals frequency shift relative to the 1MHz

frequency shift allowed by the Inficon deposition monitor. When depositing dielectric or optical materials, the life of a gold quartz monitor crystal is much shorter as much as 10 to 20% and this is due to the thermal and intrinsic stresses at the quartz-dielectric film interface²². Another reason could be the poor mechanical strength of the film and also the chamber conditions. The chamber was covered with Al foil in order to protect the chamber walls from film deposition. After running several processes the foil was all discolored because of the Ag and SiO₂ films getting deposited on them. The chamber was cleaned before the fabrication of MD stack2A and another tooling factor measurement was done prior to the fabrication of this stack.

Pre MD stack 2A Tooling measurement:

The sputter was done this time at a gas pressure of 5mTorr. The other parameters (RF, thickness) were all kept the same. The reason why the pressure was increased was because at low pressures, even though a higher rate is obtained, it may not be depositing molecules but larger sized particles and this could be a reason for the thickness variation. Also the Pirani gauge that is used in this tool which is the pressure sensor may not be sensitive at such low pressures. Figures 3.7 and 3.8 show the thickness distribution for 2000Å of Ag and SiO₂ respectively.

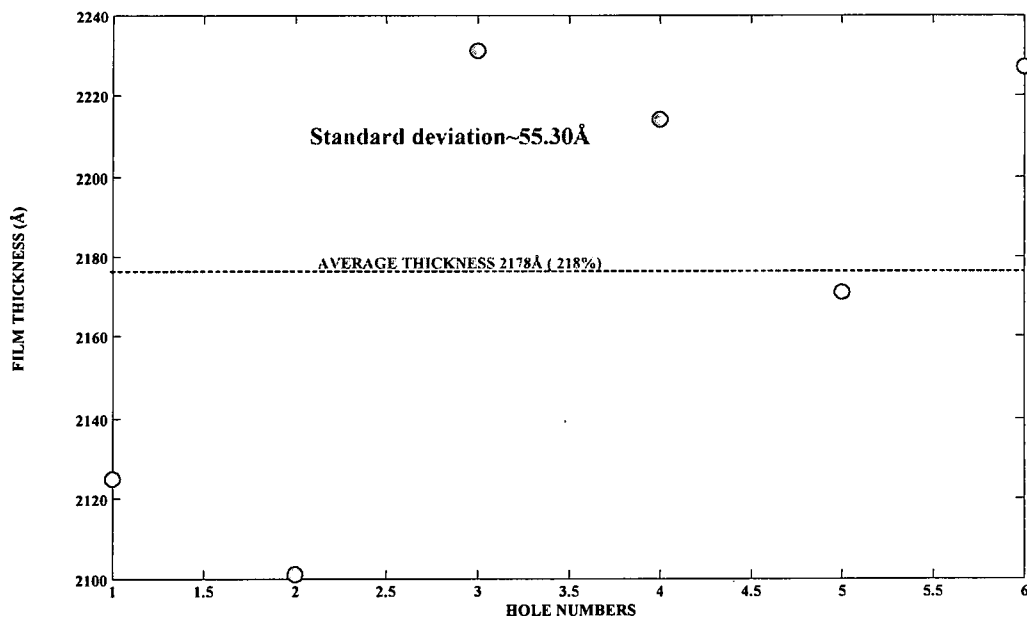


Figure 3.7 Thickness measurements across the different holes on the Ag 2000Å sample

$$T_m = 2178\text{Å}$$

$$T_x = 2001\text{Å}$$

$$TF_i = 200\% \text{ (initial estimated tooling factor)}$$

$$\text{Tooling factor (\%)} = 200 * (2178/2001) \sim 218\%$$

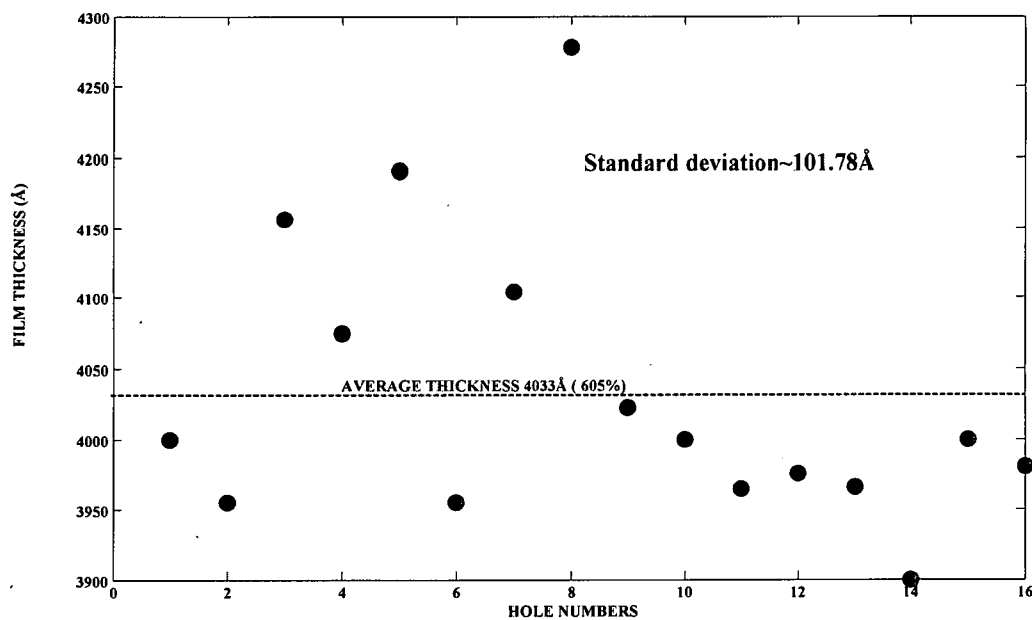


Figure 3.8 Thickness measurements across the different holes on the SiO₂ 2000Å sample

$$T_m = 4033 \text{ Å}$$

$$T_x = 2001 \text{ Å}$$

$$TF_i = 300\% \text{ (tooling factor for 2001 Å)}$$

$$\text{Tooling factor (\%)} = 300 * (4033/2001) \sim 605\%$$

It was observed that the tooling factor for SiO₂ changed very much and also the measured thickness was double the actual deposition. It was concluded that in order to get 2000Å of film, half the thickness needs to be actually deposited for a tooling factor of 303%. Based on this, MD stack 2A was fabricated.

Posts MD stack 2A Tooling measurement:

The tooling factor measurement for 2000Å of Ag and 1000Å of SiO₂ is shown in the figure 3.9 and 3.10 respectively.

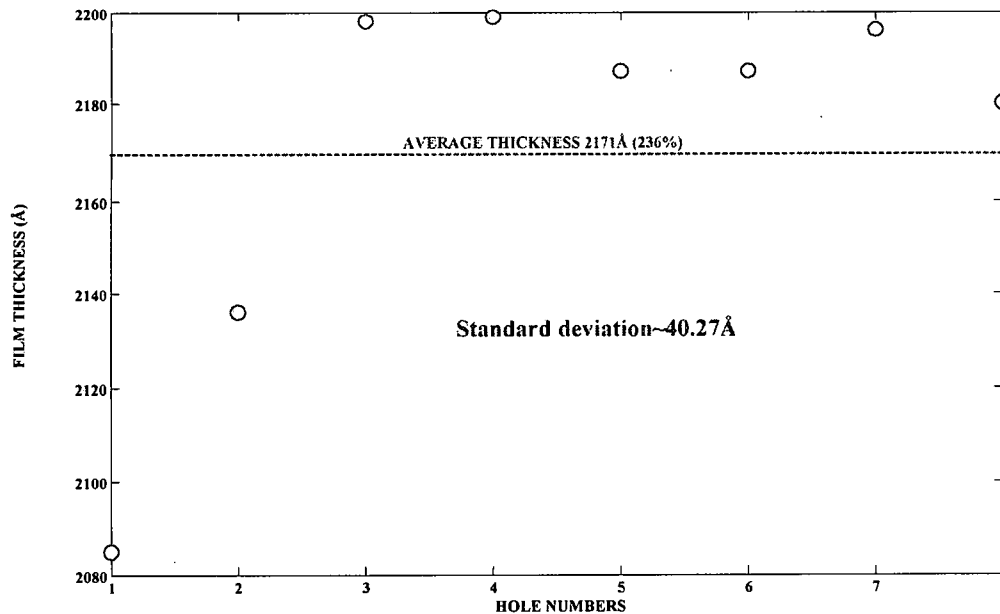


Figure 3.9 Thickness measurements across the different holes on the Ag 2000Å sample

$$T_m = 2171\text{Å}$$

$$T_x = 2002\text{Å}$$

$$TF_i = 218\% \text{ (tooling factor for } 2002\text{Å)}$$

$$\text{Tooling factor (\%)} = 218 * (2171/2002) \sim 236\%$$

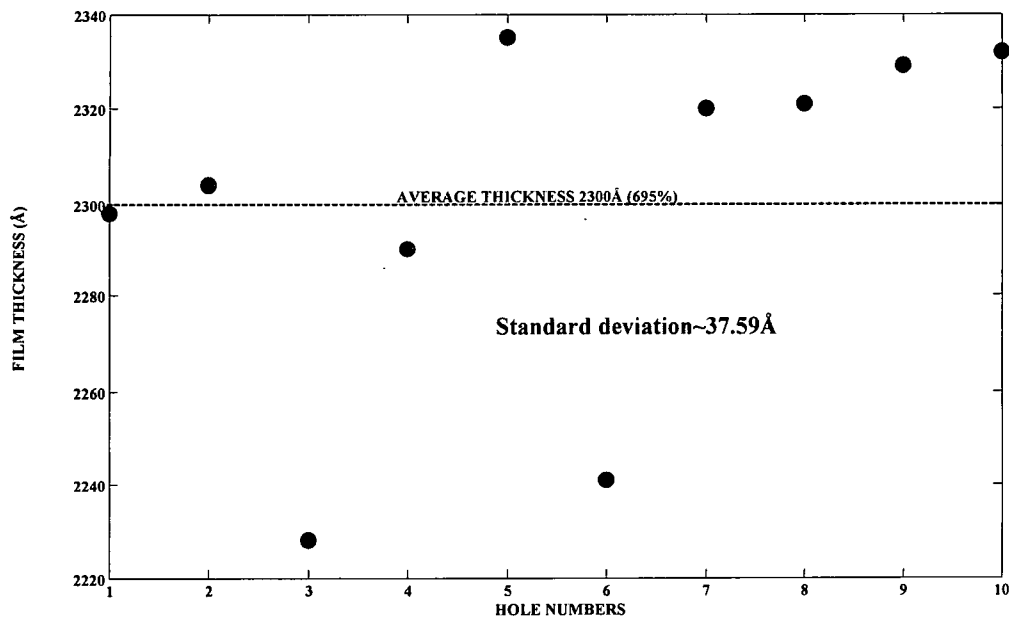


Figure 3.10 Thickness measurements across the different holes on the SiO₂ 1000Å sample

$$T_m = 2300\text{Å}$$

$$T_x = 1003\text{Å}$$

$$TF_i = 303\% \text{ (tooling factor for } 1003\text{Å)}$$

$$\text{Tooling factor (\%)} = 303 * (2300/1003) \sim 695\%$$

The results were similar to the earlier tooling factor measurement for Ag but for SiO₂ the tooling factor further increased. Based on this the 3rd MD stack was fabricated and a tooling factor measurement was done again after this. Figures 3.11 and 3.12 show the tooling factor measurement results for 2000Å of Ag and 1000Å of SiO₂ respectively after the fabrication of stack 3.

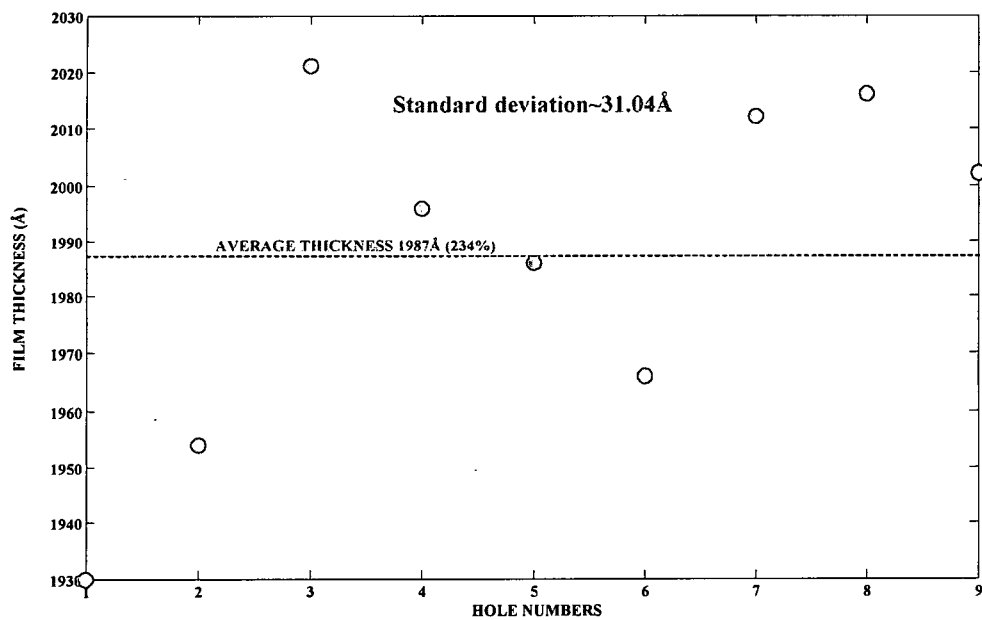


Figure 3.11 Thickness measurements across the different holes on the Ag 2000Å sample

$$T_m = 1987\text{Å}$$

$$T_x = 2001\text{Å}$$

$$TF_i = 236\% \text{ (tooling factor for } 2001\text{Å)}$$

$$\text{Tooling factor (\%)} = 236 * (1987/2001) \sim 234\%$$

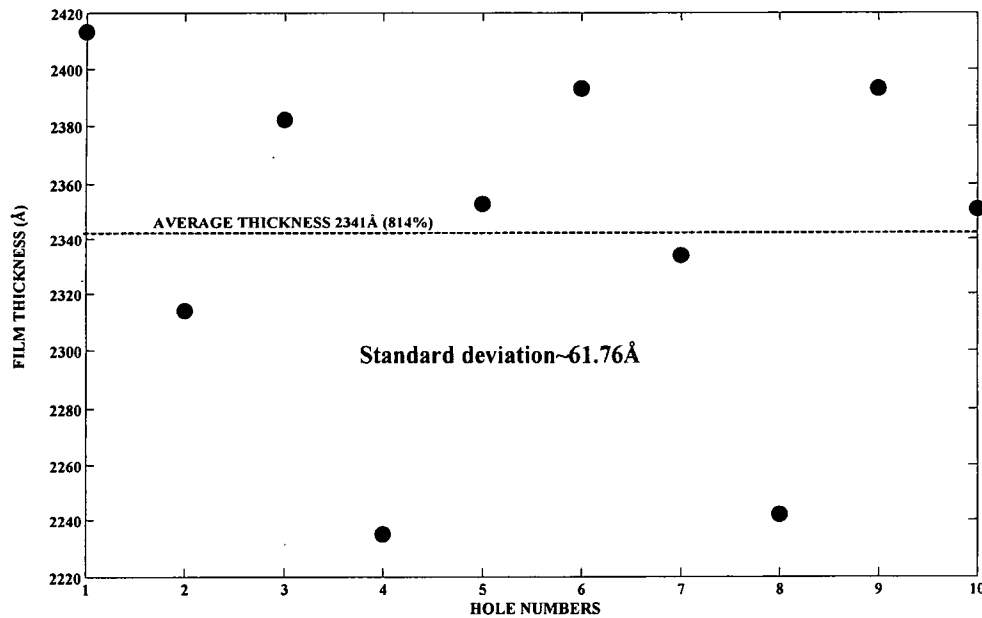


Figure 3.12 Thickness measurements across the different holes on the SiO₂ 1000Å sample

$$T_m = 2341\text{Å}$$

$$T_x = 1001\text{Å}$$

$$TF_i = 348\% \text{ (tooling factor for } 1001\text{Å)}$$

$$\text{Tooling factor (\%)} = 348 * (2341/1001) \sim 814\%$$

It was observed that the tooling factor for SiO₂ continued to keep changing and this was affecting the stack thickness measurements too which will be discussed in the chapter on Metallo dielectric stacks, chapter IV. Every time SiO₂ was deposited, there were yellow particulates in the chamber especially on the shutter and the target sleeve. These yellow particulates were formed as a result of the O₂ that was liberated due to ionization. It is actually O₂ deficient SiO₂. It is SiO_{2-x} ie, SiO (Silicon Monoxide). Only some valence electrons were getting stripped off from the outer most shell of SiO₂. As a result, the film

that was being deposited was not pure SiO_2 . In order to avoid this SiO formation, 4%-6% of O_2 should also be bled into the chamber along with the process gas (Ar here) to recover the SiO_2 stoichiometry. X-Ray Diffraction study of the sample deposited with SiO_2 will give the right amount of O_2 that needs to be released into the chamber along with Ar. This was not pursued under this study.

Study of Argon Gas Pressure Vs Deposition Rate and Tooling

As the argon gas pressure increases, the number of ions colliding on the target increases thus increasing the deposition rate as shown in figure 5.13. If the gas pressure is increased further, the sputter rate drops as now there are too many argon ions and they collide with each other and hence do not reach the target.

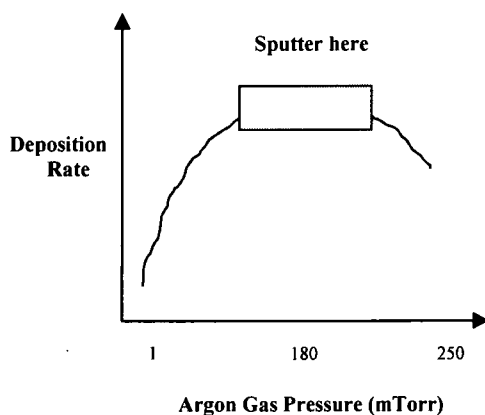


Figure 3.13 Argon gas pressure Vs Deposition rate ($\text{\AA}/\text{s}$)¹⁷

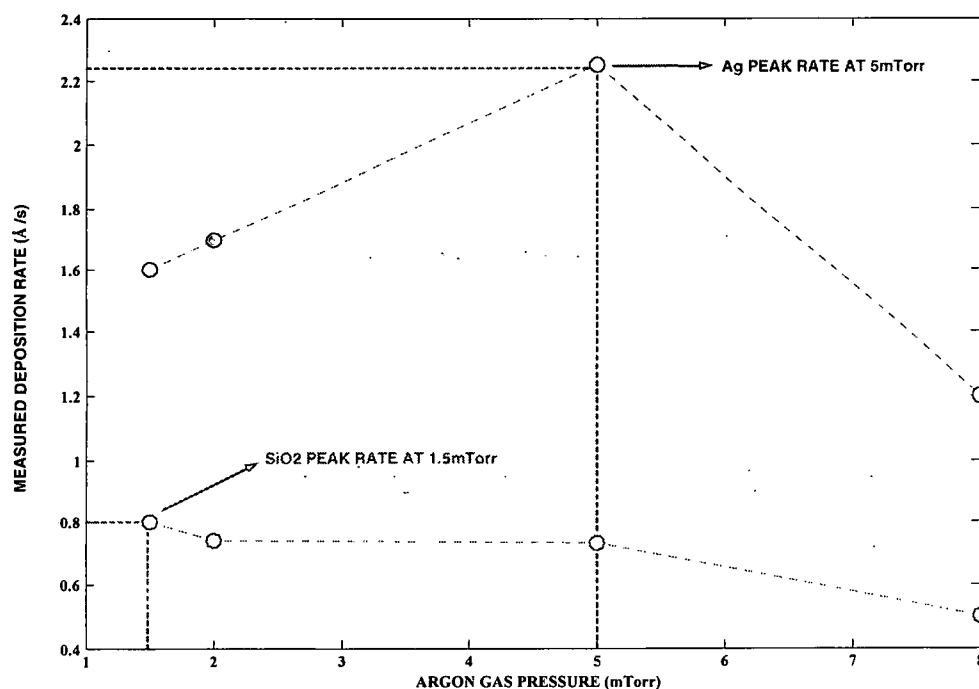


Figure 3.14 Argon Gas pressure Vs Measured Deposition Rate for Ag & SiO₂

Figure 3.14 shows the variation of measured deposition rate with various gas pressures for Ag and SiO₂. The above study was done at an RF power of 50W for Ag and 300W for SiO₂. As the deposition rate is independent of thickness, it was not kept a constant. Also since the tooling factor did not always remain constant, the deposition rate was measured by first depositing 1000Å or 2000Å of Ag or SiO₂ film on a glass substrate and then measuring the thickness using the Ambios XP profiler and from this measured thickness a new tooling factor was calculated. The deposition time was monitored and the new rate was calculated as shown below,

Measured thickness for 1003Å of SiO₂ = 754Å

Initial estimated tooling factor = 299%

Measured Tooling factor = $299 \times (754/1003) = 225\%$

Measured Deposition Time = 953s; Measured Deposition Rate = $754/953 = 0.8 \text{ \AA/s}$

The same method was followed to calculate the rates for Ag at various gas pressures. It was found that the maximum rate for silver was 2.25 \AA/s at 5mTorr and that for SiO_2 was 0.8 \AA/s at 1.5mTorr. Though the RF for SiO_2 was greater than Ag the rate was lower because the electrical/thermal conductivity of SiO_2 is very low. Thus we concluded that the maximum sputter rate for different materials change with the process gas pressure. Another important result of this study is shown in figure 3.15, that the measured tooling factor changes at different gas pressures for different materials.

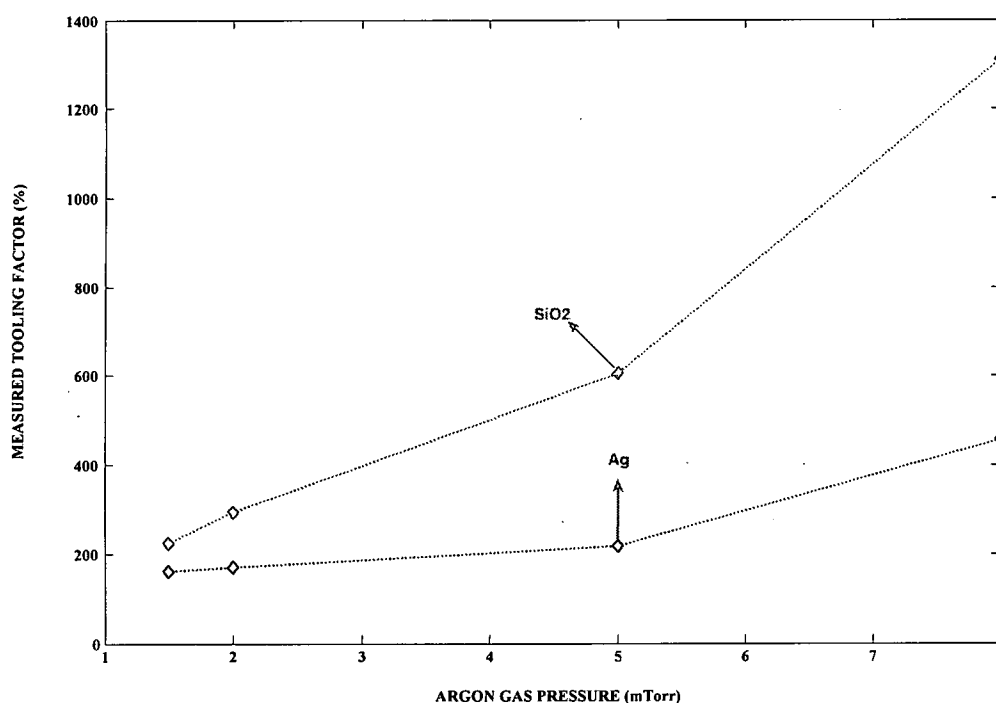


Figure 3.15 Argon Gas Pressure Vs Measured Tooling

It was observed that as the measured tooling factor for Ag is almost a constant up to 5mTorr but beyond that the tooling factor increases. For SiO_2 the tooling factor increases

considerably for various gas pressures. This implies that as the gas pressure is increased to beyond a certain value, large chunks of the material are deposited and this affects the thickness of the film as now the film is very rough and the deposition is more directional and more film gets deposited on the substrate than the crystal monitor this in turn changes the tooling factor.

Thin Film Stress Measurement^{12, 23}

Stress in Deposited Layers: A thin film deposited on a substrate can be either in tensile stress, in which the film would relax by contracting, or it may be in compressive stress. If the stress in the film is too large, the film may peel from the surface of the wafer. The film stress and structure play important roles in the performance, and particularly in the reliability, of the films. Large stress may give rise to void formation upon subsequent thermal cycling. One component of stress is caused by thermal expansion mismatch of the film with the substrate. This stress is seen when the deposition is not done at room temperature. If E is the Young's modulus for the material and ν is the Poisson's ratio, and it is assumed that E and ν are temperature independent, this stress is given by,

$$\sigma_{th} = \frac{E_{film}}{1 - \nu_{film}} \int_{T_0}^{T_{dep}} (\alpha_{film} - \alpha_{sub}) dT$$

Films may form single crystal grains during the deposition process. For polycrystalline films, stress can arise when the deposition is carried out at high temperature. Under these conditions, the larger grains grow at the expense of the smaller grains. The increase in the crystalline order will lead to an overall stress. The intrinsic stress depends on the substrate temperature, deposition rate, film thickness, and background chamber ambient. If the deposition is carried out at low temperature, the intrinsic stress is small.

The total stress in a thin film takes into account both these stresses.

$$\sigma = \sigma_{th} + \sigma_{bi}$$

Stress in a film is commonly measured using the change in the bow of the wafer before and after film deposition as shown in figure 3.16.

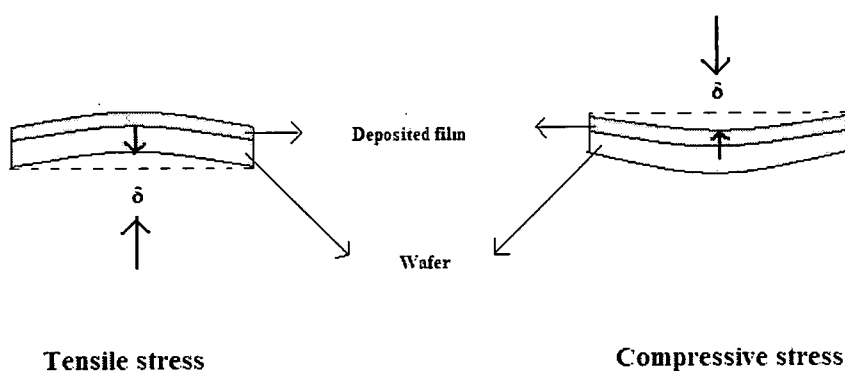


Figure 3.16 The change in wafer deflection may be used to measure the stress in a deposited layer¹².

Thin film stress is given by,

$$\sigma = \frac{\delta}{t} \frac{E}{1-\nu} \frac{T^2}{3R^2}$$

Where δ is the change in the deflection of the center of the wafer, t is the film thickness, R is the radius of the wafer, and T is the thickness of the wafer.

The Wafer Stress Option, in the Ambios XP determines the stress levels in a deposited film by measuring the deflection or curvature that the stress induces in the substrate. The

software determines the curvature of the sample by calculating the least square fit of the trace data to a circle. The equation for stress is as follows:

$$\sigma = [1/6R] [E/(1-\nu)] [t_s^2/t_f]$$

Where:

$E/(1-\nu)$ = substrate elastic constant

E = Young's Modulus

ν = Poisson's Ratio

t_s = substrate thickness

t_f = film thickness

R = radius of curvature

The software calculates the radius of curvature by using a least squares fit method. It is actually the difference between the prestress data (plain glass substrate) and the post stress data (substrate after the film deposition).

The XP software uses manually entered values for t_s (glass substrate thickness is $0.155\text{mm} \pm 0.005\text{mm}$) and t_f (film thickness).

Stress Type – The software uses the Stoke's Model for calculating the stress based on the curvature of the profile. The results are categorized as either Compressive or Tension Stress types.

Average Stress (MPa, Mega Pascal) – This field displays the calculated average stress of the film on the substrate for the length of the profile data.

Center Stress (MPa) - This field displays the calculated stress of the film on the substrate at the center of the profile data.

The stress measurements for this particular study were done for two different thicknesses for Ag and SiO₂. Table 3.2 and Table 3.3 shows the stress measurements for 1000Å and 5000Å of silver respectively.

Table 3.2 Stress Measurements for 1000Å of Ag on a glass substrate

Trials	Stress Type	Average Stress(MPa)	Center Stress(MPa)
1	Tensile	47	15.9
2	Tensile	108	18.5
3	Compression	47.4	526.7
		100.1	410.3
4	Tensile	304.8	524.6
		408.4	332.6

Table 3.3 Stress Measurements for 5000Å of Ag on a glass substrate

Trials	Stress Type	Average Stress(MPa)	Center Stress(MPa)
1	Compression	41.3	97.4
		53.7	81.6
2	Tensile	89	99.9
3	Tensile	185.3	163.7
4	Tensile	87.7	83.9

The study showed two different kinds of stresses on Silver. The sample was measured in the same location and with the same scan sequence to produce accurate and repeatable

stress measurements using the difference measurement method. The sample was marked before the stress measurement was carried out and post stress measurements were carried through the same points. Also the same scan sequence was used for all the stress measurements.

Scan Parameters:

Scan Speed 0.1mm/sec

Scan length 15mm

Height Range 100 μ m

Stylus Force 2 mg

Filter level²³ 3- This defines the number of data points that will be plotted in the profile.

The number is defined as 2^x , where the x is the number in the software field. The filter values are from 0-5. A value of 0 will have no filtering. A value of 3 will divide the data points by 8 and average the 8 data points then plot this average value for each group of 8 data points. The instrument always acquires data at 2000 points/sec.

Table 3.4 and Table 3.5 shows the stress measurements for 1000Å and 3000Å of SiO₂ respectively.

Table 3.4 Stress Measurements for 1000Å of SiO₂ on a glass substrate

Trials	Stress Type	Average Stress(MPa)	Center Stress(MPa)
1	Compression	291.1	555.4
		366	357.3
2	Compression	190.3	189.1
3	Compression	112.6	27.8
4	Compression	57.4	241.4

Table 3.5 Stress Measurements for 3000Å of SiO₂ on a glass substrate

Trials	Stress Type	Average Stress(MPa)	Center Stress(MPa)
1	Compression	210.1	182.7
2	Compression	392.5	609.1
3	Compression	343.4	280.3
4	Compression	221.0	175.6

It was observed that Ag has different kinds of stresses on the same sample. On the other hand SiO₂ had the same kind of stress on the entire sample. The stress depends primarily on the substrate used. The glass substrate that was used in this study already had a bow to it. Also the film depending upon the kind of material that is being deposited adds an extra stress to the substrate. The Ambios software actually uses the second derivative of the bow to calculate the stress. When the software (using Stoke's model) finds the difference between the pre and post stress data and if this difference leads to a convex result, then it shows a tensile stress and if it leads to a concave result, then it shows a compression stress. The reason for Ag film having two different kinds of stresses on it could be because, when the film is deposited on the glass substrate, some part of the substrate could be under tensile stress and some under compression stress. So the difference leads

to these two different stresses on the substrate. On the other hand, SiO_2 has the same kind of stresses on it may be because the elastic constants of the substrate and SiO_2 match as they both are glass materials and hence compensates for the different curvatures on the substrate after the film deposition.

Thin Film Roughness Measurement^{10,11}

Real surfaces are not flat on an atomic scale. Surface roughness that is associated with thin-film deposition has a direct effect on the performance of solid-thin film devices. For thin films that are prepared for optical waveguides, multilayer interference filters, and optical resonant filters, surface roughness becomes a significant issue.

In this present study, surface roughness measurements were done on 1000Å and 2000Å of sputtered Ag and SiO_2 films using the Ambios profiler. The Ambios Technology XP software separates the waviness and roughness components of the data by selecting a Cutoff Filter. The Filters provide an adjustable short wave cutoff filter and isolates wavelengths. In this study, roughness was measured at different cutoff values and for different RF powers. The materials were sputtered at a gas pressure of 2mTorr for Ag and 1.5 mTorr for SiO_2 . Figure 3.17 shows the average roughness for 1000Å of Ag and SiO_2 deposited on a silicon wafer (flat surface).

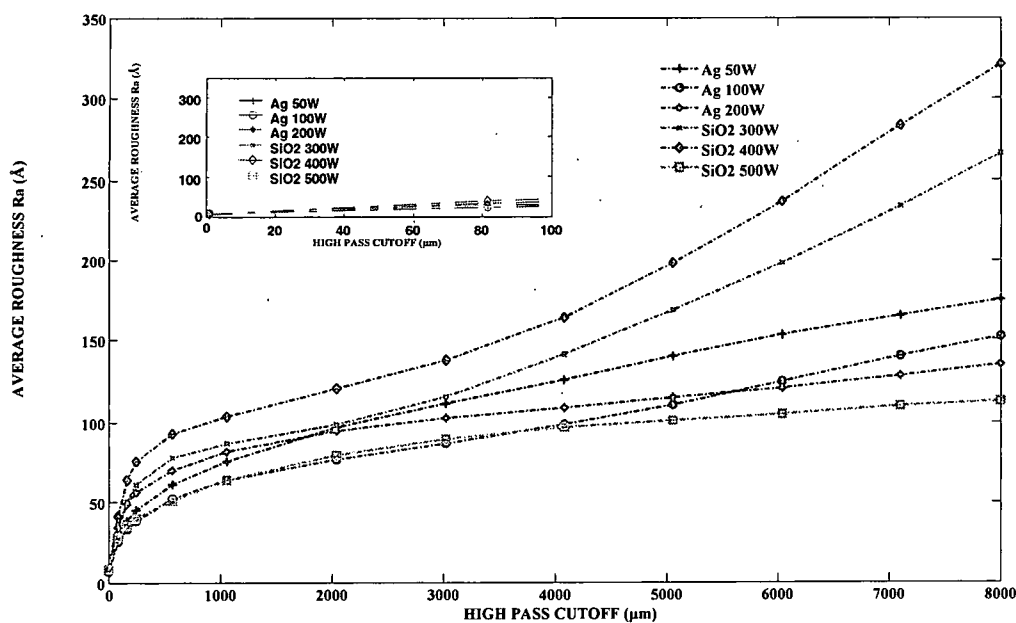


Figure 3.17 Average roughness, Ra measurement for 1000Å of Ag and SiO₂

Average Roughness Ra (filtered) — is the arithmetic average of the absolute values of the profile height deviations recorded within the evaluation length (L) and measured from the mean line. $R_a = (|Z_1| + |Z_2| + |Z_3| \dots |Z_N|)/N$.

The roughness was measured at several different RF powers. 50W, 100W and 200W for Ag and 300W, 400W and 500W for SiO₂. The RF sputter power for SiO₂ is different because at 50W, the rate was just 0 Å/s because of its poor sputter yield. In order to get a higher rate the RF power was increased. The average roughness for Ag was slightly greater at 50W and SiO₂ was greater for 400W. Figure 3.18 shows the RMS roughness for 1000Å of Ag and SiO₂ deposited on a silicon wafer (flat surface).

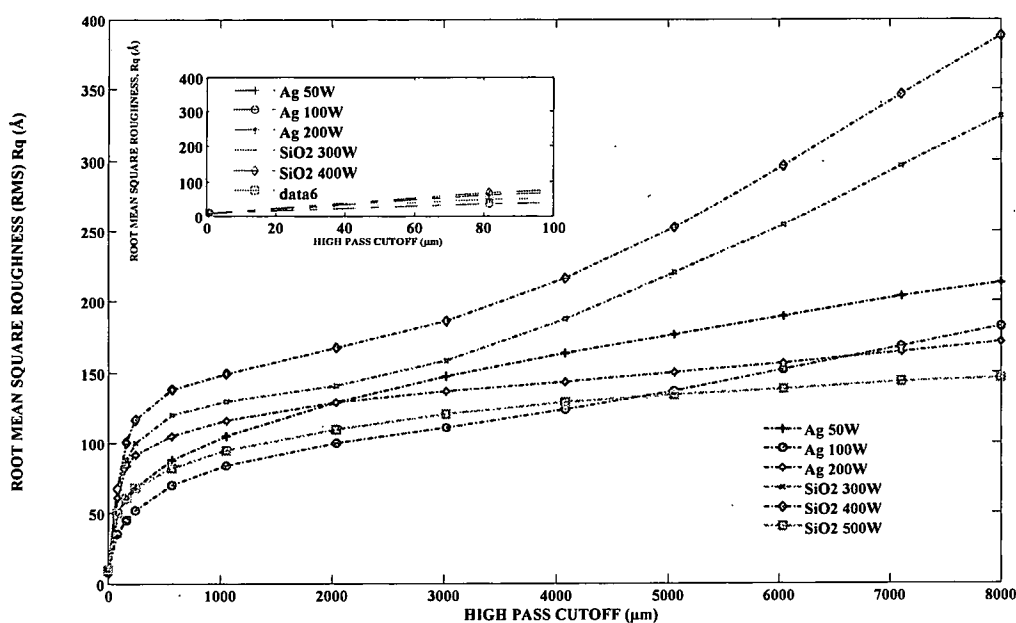


Figure 3.18 Root Mean Square roughness, Rq measurement for 1000Å of Ag and SiO₂

Root Mean Square Roughness (RMS) Rq (filtered) — is the root mean square average of the profile height deviations taken with the evaluation length (L) and measured from the mean line. $R_q = [(Z_1^2 + Z_2^2 + Z_3^2 + \dots + Z_N^2)/N]^{1/2}$.

The RMS roughness is almost the same at different RF powers but the roughness for SiO₂ at 400W is greater than Ag. Figure 3.19 shows the Roughness (Peak-Valley) for 1000Å of Ag and SiO₂ deposited on silicon wafer (flat surface).

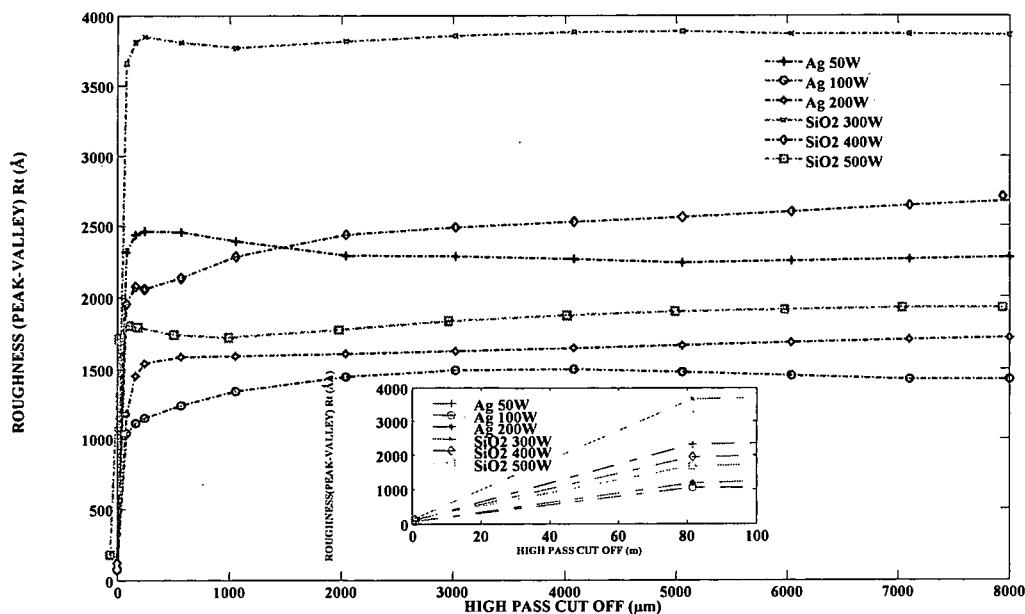


Figure 3.19 Roughness (Peak – Valley) Rt measurement for 1000Å of Ag and SiO₂

Roughness (Peak – Valley) Rt (filtered) – The P-to-V is a measurement of the lowest point to the highest point of the profile from the center-line of the R (reference) cursor to the centerline of the M (measurement) cursor.

The roughness for SiO₂ at 300W was the maximum in comparison to Ag. The study of roughness at different RF powers enabled the conclusion that there is not much of a difference in roughness for Ag and SiO₂ at different RF powers. RF power is not a major factor in determining the roughness of thin films but it is something else like substrate temperature and thickness of the film deposited. During the coalescence stage of the thin film growth process, in which small islands start coalescing with each other in an attempt to reduce the surface area, the tendency to form bigger islands is enhanced by increasing the surface mobility of the adsorbed species by increasing the substrate temperature. By

controlling the substrate temperature we increase the mobility of these molecules forming these islands and as a result it fills up the uncovered holes on the substrate resulting in a continuous film. This happens at small thicknesses but at large thicknesses the growth of coarse-grained rough films becomes continuous. Here again, smooth films can be obtained by increasing the substrate temperature¹³.

CHAPTER IV

METALLO DIELECTRIC STACKS

The technology of multi-layered thin films is essential for a variety of optical structures, such as optical filters, anti-reflection coatings and photonic band gap structures. These structures take advantage of combinations of materials with differing indices of refraction in a periodic fashion to obtain novel transmission and reflection properties. The large index contrast between metals and dielectrics can be utilized to produce very broad reflection spectra (and correspondingly wide stop bands) using substantially fewer layers compared to all dielectric periodic structures. Furthermore, despite the high absorption coefficient of the metal films, a high transmission coefficient could be achieved by carefully placing the metal films at the field minima of the resonant wave.

One-dimensional PBG structures consist of the alternation of two different materials having high (nH) and low (nL) refractive index, respectively, with layer thicknesses of the order of optical wavelength. Two different consecutive layers form one period. The main features of the resulting structure can be summarized as follows: some wavelength ranges are completely reflected, giving rise to so called band gaps, while other wavelength ranges are nearly completely transmitted (passbands), and the transmission spectra shows strong oscillatory behavior in the form of Fabry-Perot like resonances. For a N -period structure, there are $2N-1$ resonances between consecutive gaps, and the

bandwidth of transmission resonances and the width of the band gap depend on N and on the index contrast $nH - nL$.

Figure 4.1 shows the reason as to why a periodic metallo dielectric structure is preferred to a single metal layer.

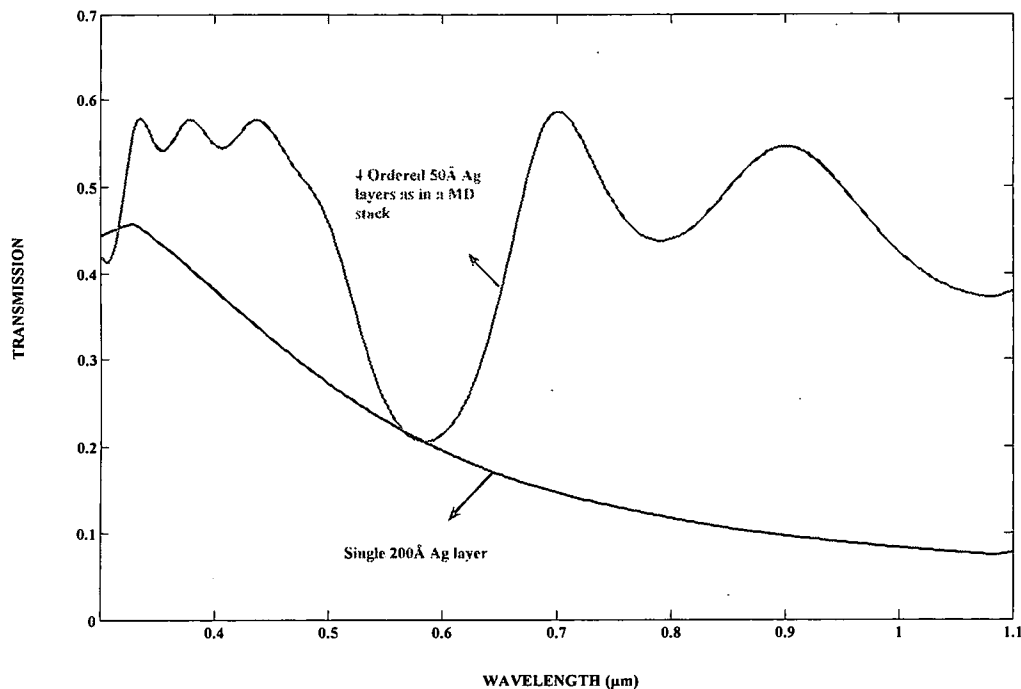


Figure 4.1 Wavelength (μm) Vs Transmission model

The model was designed using the TMM program. When a single Ag layer of 200\AA is used, it was observed that the transmission decreases in the visible region as the metal layer absorbs the entire light incident on it. But on the other design, 4 ordered layers of 50\AA of Ag showed a increase in the transmission property of the structure as now metal layers are placed in the field minima as shown in the figure 4.2 and this decreases the absorption and increases the transmission.

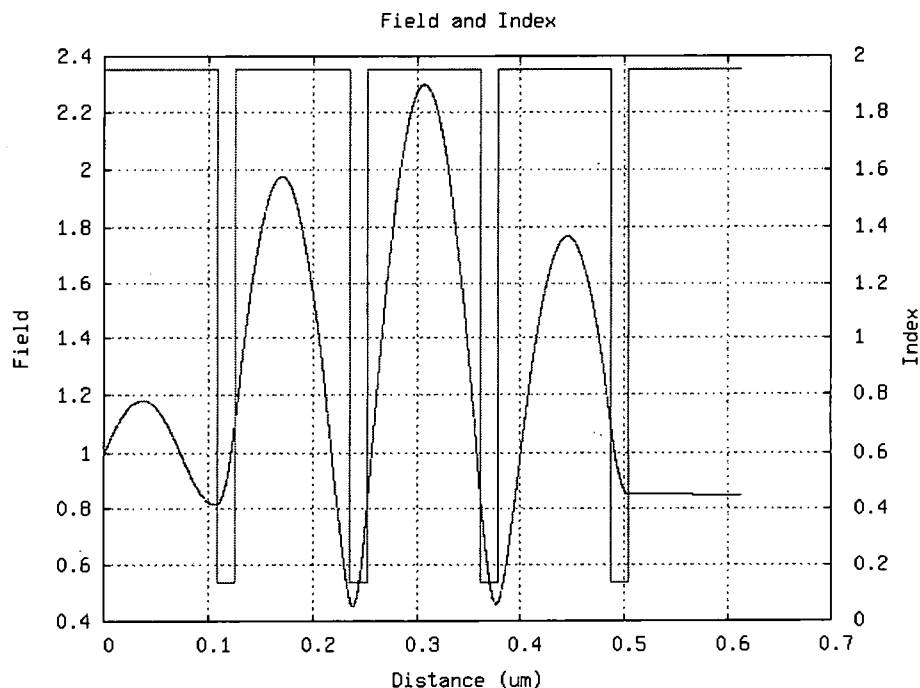


Figure 4.2 Field Profile for the MD stack

With these considerations in mind, 5 different metallo dielectric stacks were fabricated containing 4 pairs of metal (Ag) layers due to the low refractive index value typically offered by metals in the visible range and SiO_2 (dielectric) layers by varying the various sputter parameters and thicknesses of these materials. In MD-PBGs, the electromagnetic field at frequencies below the metal plasma frequency is strongly confined into the dielectric layers, due to the high reflective properties of the metal. Moreover, a resonant tunneling mechanism allows appreciable transmission values, despite the high nominal absorption of the light in the metal layers¹.

Transfer Matrix Method (TMM)^{20, 25}

The multilayer metallodielectric interference films were designed using the transfer matrix method (Figure 4.3). The TMM is a powerful tool for the analysis of periodic structures. It can be used in two different ways. One way is to represent the solution of the coupled mode equations (perturbation analysis) by a 2×2 transfer matrix, which relates the forward and backward propagating field amplitudes. Almost periodic gratings can be analyzed effectively by this method. The grating structure is divided into a number of uniform grating sections which have an analytic transfer matrix. The transfer matrix for the entire structure is obtained by multiplying the individual transfer matrices together.

The other way of the TMM is to represent each layer by a transfer matrix. The reflection of the propagating modes of a corrugated waveguide at the discontinuity of the corrugation can be described by the discontinuity of the effective index in the same way as plane waves are reflected. The transfer matrix of each corrugation can be expressed in terms of the continuity of the field and its derivative across the boundaries.

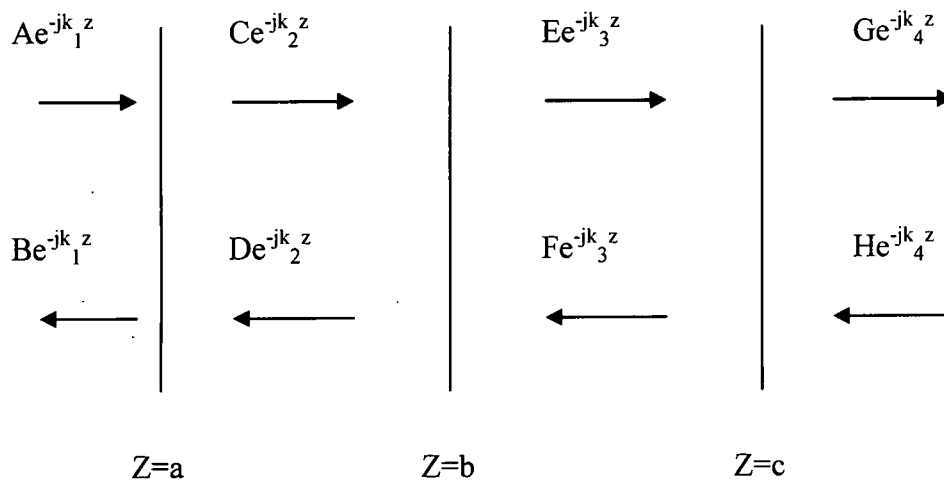


Figure 4.3 Transfer Matrix Method²⁰

Using the latter approach,

$$\begin{bmatrix} e^{-jk_1 a} & e^{jk_1 a} \\ -jk_1 e^{-jk_1 a} & jk_1 e^{jk_1 a} \end{bmatrix} \begin{bmatrix} A \\ B \end{bmatrix} = \begin{bmatrix} e^{-jk_2 a} & e^{jk_2 a} \\ -jk_2 e^{-jk_2 a} & jk_2 e^{jk_2 a} \end{bmatrix} \begin{bmatrix} C \\ D \end{bmatrix} \quad 6.1$$

and

$$\begin{bmatrix} e^{-jk_2 b} & e^{jk_2 b} \\ -jk_2 e^{-jk_2 b} & jk_2 e^{jk_2 b} \end{bmatrix} \begin{bmatrix} C \\ D \end{bmatrix} = \begin{bmatrix} e^{-jk_3 b} & e^{jk_3 b} \\ -jk_3 e^{-jk_3 b} & jk_3 e^{jk_3 b} \end{bmatrix} \begin{bmatrix} E \\ F \end{bmatrix} \quad 6.2$$

This can be written as:

$$M_1(a) \begin{bmatrix} A \\ B \end{bmatrix} = M_2(a) \begin{bmatrix} C \\ D \end{bmatrix} \quad 6.3$$

where

$$M_n(z) = \begin{bmatrix} e^{-jk_n z} & e^{jk_n z} \\ -jk_n e^{-jk_n z} & jk_n e^{jk_n z} \end{bmatrix} \quad 6.4$$

Similarly,

$$M_2(b) \begin{bmatrix} C \\ D \end{bmatrix} = M_3(b) \begin{bmatrix} E \\ F \end{bmatrix} \quad 6.5$$

This result in

$$M_1(a) \begin{bmatrix} A \\ B \end{bmatrix} = M_2(a) M_2^{-1}(b) M_3(b) \begin{bmatrix} E \\ F \end{bmatrix} \quad 6.6$$

$$M_3^{-1}(b) M_2(b) M_2^{-1}(a) M_1(a) \begin{bmatrix} A \\ B \end{bmatrix} = \begin{bmatrix} E \\ F \end{bmatrix} \quad 6.7$$

For a structure with N layers, we can write

$$M_N^{-1}(z_N) M_{N-1}(z_N) \circ \circ \circ M_3^{-1}(b) M_2(b) M_2^{-1}(a) M_1(a) \begin{bmatrix} A \\ B \end{bmatrix} = \begin{bmatrix} Y \\ Z \end{bmatrix} \quad 6.8$$

which can be simplified as

$$T \begin{bmatrix} A \\ B \end{bmatrix} = \begin{bmatrix} Y \\ Z \end{bmatrix} \quad 6.9$$

where Y and Z and the field amplitudes in the last layer, and T is the product of all the individual matrices.

Since the left traveling wave in the last layer is typically zero, if we assume the incident field to have an amplitude of 1, we can write:

$$T \begin{bmatrix} 1 \\ r \end{bmatrix} = \begin{bmatrix} t \\ 0 \end{bmatrix} \quad 6.10$$

where t and r are the field transmission and reflection coefficients respectively.

Therefore,

$$\begin{bmatrix} T_{11} & T_{12} \\ T_{21} & T_{22} \end{bmatrix} \begin{bmatrix} 1 \\ r \end{bmatrix} = \begin{bmatrix} t \\ 0 \end{bmatrix} \quad 6.11$$

$$T_{21} + T_{22}r = 0 \quad 6.12$$

$$r = -\frac{T_{21}}{T_{22}} \quad 6.13$$

Similarly,

$$T_{11} + T_{12}r = t \quad 6.14$$

$$t = T_{11} - \frac{T_{12}T_{21}}{T_{22}} \quad 6.15$$

Dispersion profile for Ag and SiO₂

Single layers of Ag and SiO₂ were optically characterized by spectrophotometry, in order to derive the refractive index and absorption curves^{1, 14}. Figure 4.4 and 4.5 shows the dispersion profiles for Ag and SiO₂ respectively.

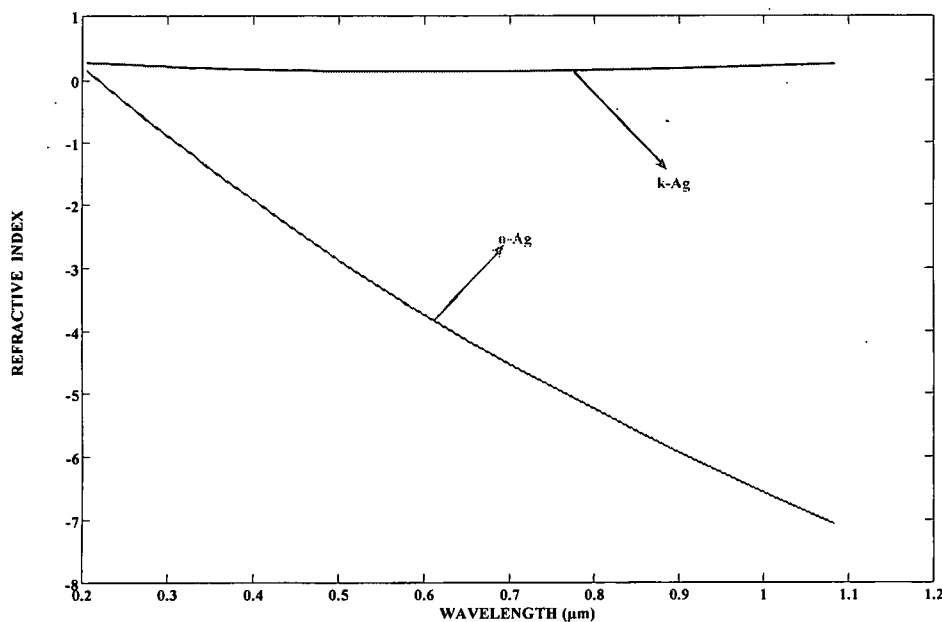


Figure 4.4 Dispersion profile for Ag

The real, $n(\lambda)$ and the imaginary, $k(\lambda)$, components of the refractive index have been derived by fitting the data according to a Fabry - Perot model applied to a linearly absorbing layer^{1, 5}. For Ag, $n(\lambda)$ and $k(\lambda)$ were obtained by using the following equations,

$$n(\lambda) = -0.341.\lambda^3 + 1.37.\lambda^2 - 1.3.\lambda + 0.492$$

$$k(\lambda) = 1.41.\lambda^3 - 6.12.\lambda^2 + 14.1.\lambda - 2.82$$

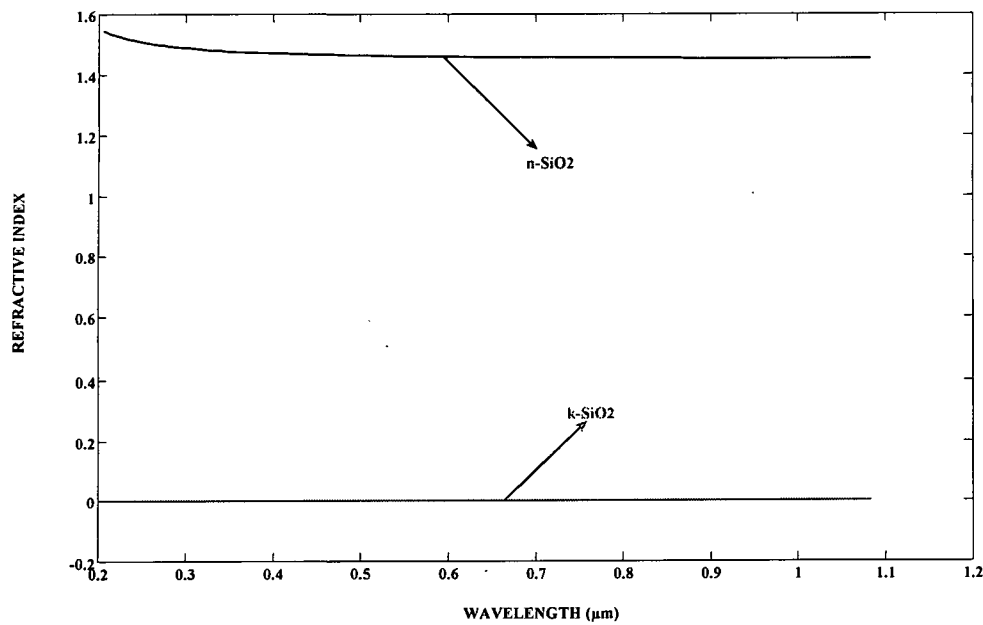


Figure 4.5 Dispersion profile for SiO₂

For SiO₂ the $n(\lambda)$ values were obtained from the book on optical constants¹⁴ and the $k(\lambda)$ values were obtained from the following equation,

$$k(\lambda) = \frac{A\lambda}{4\pi \log e}$$

where A is the absorption value obtained at different wavelengths from the spectrophotometer scan and t is the thickness of glass substrate (155 μm). Since the SiO₂ refractive index is greater than the metal layer, it is possible to confine light in this layer.

MD (Metallo- Dielectric) stack-1

The very first stack was fabricated based on the theoretical model which was designed using the LIGHTS, TMM software. It consisted of 5 layers of SiO₂ (2576 Å) and 4 layers of Ag (170 Å). The stacks were fabricated at 2mTorr gas pressure and the sputtering was

done at 50W for Ag and 300W for SiO₂. The reason for choosing a gas pressure of 2mTorr was because when a rate study was done based on different gas pressures we got the maximum rate for Ag and SiO₂ at this pressure. Since during this fabrication, the profiler was not yet available as a result the thickness of this stack could not be measured. After the stacks were fabricated, a UV visible spectrophotometer as shown in figure 4.6 was used to study for the transmission at different wavelengths in the visible region.

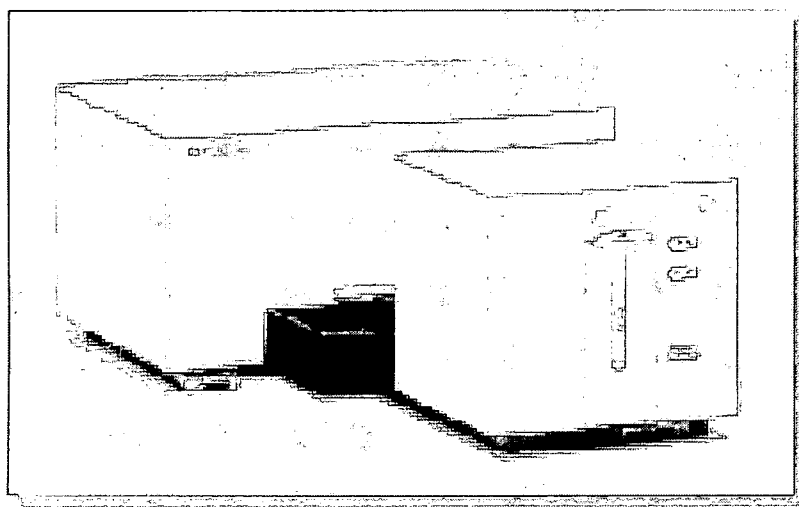


Figure 4.6 UV visible spectrophotometer²¹

Absorbance is the default method of spectral storage in the UV-visible Chemstation. In order to obtain the transmittance from the Absorbance, the following equation was used,

$$T = 100 * 10^{(-A)}$$

Where A is the Absorbance and T is the Transmittance in percent. After obtaining the measured data using the spectrophotometer, the measured result was fit onto the theoretical model. Figure 4.7 shows the result for MD stack-1.

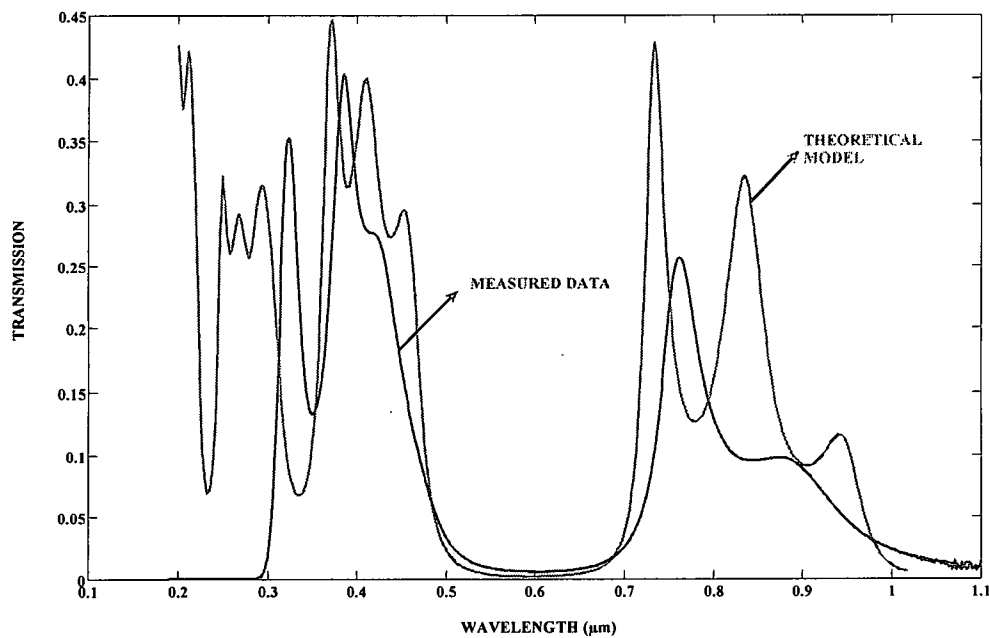


Figure 4.7 Fitting the measured data onto the theoretical model for stack-1

It was observed that the measured data showed a transmission of around 25% in the visible region as compared to the model which showed a transmission of more than 40%. Also there was mismatch between the transmission peaks of the measured and the theoretical model. The band gap was between 500nm to 700nm and the band gap matched pretty well with the model.

In order to arrive at the right thickness for the SiO₂ and Ag layers, several designs were simulated and finally it was concluded that the

- Center wavelength is determined by SiO₂ alone which is half wavelength thick ($\lambda/2n$) i.e., 2000Å
- Thicker Ag film has greater IR attenuation, but also greater visible attenuation. In order to have higher transmission in the visible region, the Ag film thickness should be small, somewhere around, $\lambda/400n$

- Smaller metal loss has smaller fundamental resonance, but higher order resonances are stronger. Increasing the metal loss increases the resonance of the fundamental.

Based on these conclusions, there were three designs that were simulated and each had a SiO₂ thickness of 2000Å and the Ag thickness was 80Å and 50Å.

MD (Metallo- Dielectric) stack-2

Since the performance of metallo-dielectric structures is greatly influenced by the uniformity, surface roughness and stress of the thin films, as was discussed in the earlier chapter, careful calibration and characterization of the films is an essential step in the fabrication process. With these parameters in mind, the films thicknesses were calibrated before the fabrication of stacks and after the fabrication as well. Stack-2 was fabricated with 4 pairs of Ag and SiO₂ layers. 80Å of Ag was sputtered at 50W and at a process pressure of 2mTorr with a measured tooling value of 178% and 2000Å of SiO₂ was sputtered at 300W and at a process pressure of 1.5mTorr with a measured tooling factor of 217%. Figure 4.8 shows a linearly tapered stack which was modeled using the pre and post tooling factors. Figure 4.9 shows a comparative study of the measured and the theoretical model.

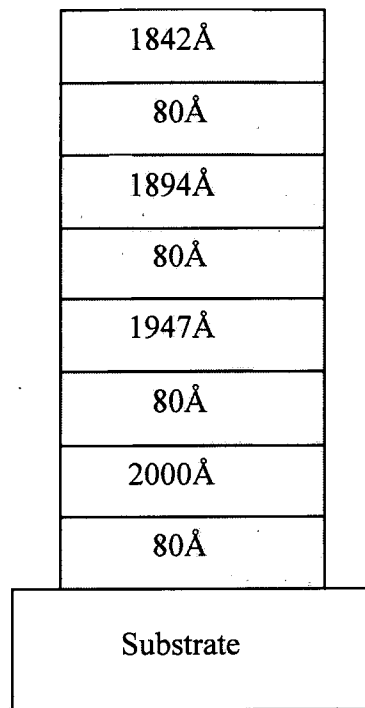


Figure 4.8 Tapered model of stack-2

The SiO_2 layers in the design were tapered as shown in the figure based on the new thickness for SiO_2 that was calculated after the stack fabrication.

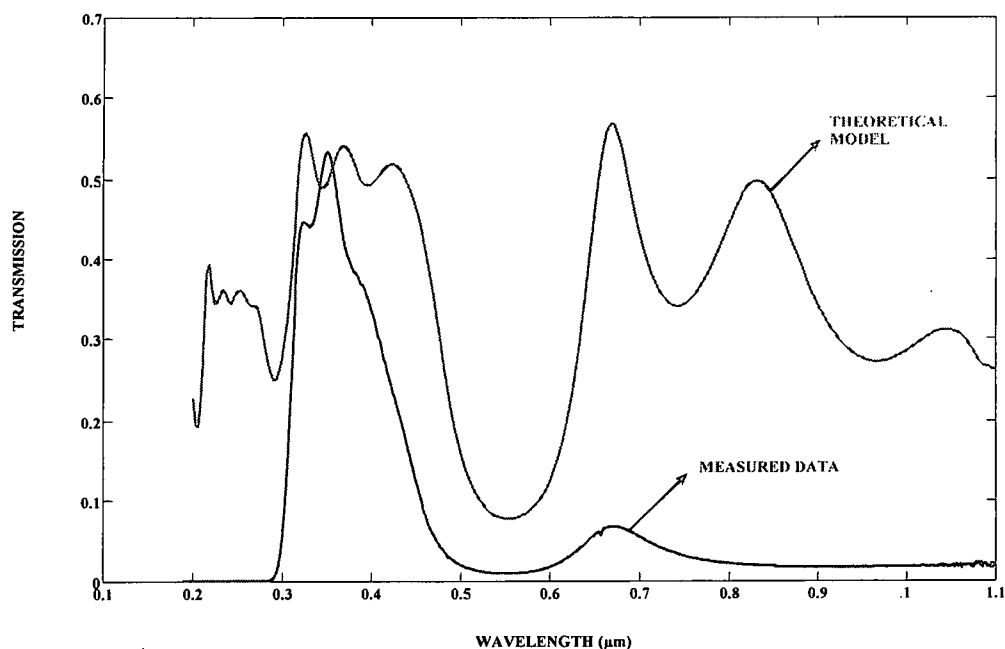


Figure 4.9 Fitting the measured data onto the theoretical model for stack-2

It was observed that the transmission of the stack was much lower in the long wavelengths. Also there the match between the measured data and the theoretical model was not nearly as good. The new measured tooling factor after the fabrication of this stack was 181% for Ag and 200% for SiO_2 . The tooling factor for SiO_2 decreased and for Ag it increased. Also on opening the chamber the Al foil was all black as it was coated with AgO. It was concluded that the O_2 molecule in the moisture reacted with the Ag atoms and was responsible for the deposition of AgO on the walls of the chamber. The chamber was cleaned and the tooling factor was calculated again. This time the tooling factor for Ag was 218% and for SiO_2 it was 605%. Also it was noticed that after sputtering Ag the chamber walls had not turned black and it was concluded that Ag was actually combining with the O_2 that was released by SiO_2 when it was sputtered and

stack-2 must have had AgO (silver oxide) instead of Ag and this could be why the stack was all messed up.

MD (Metallo- Dielectric) stack-2A

This stack was fabricated with 4 pairs of Ag and SiO₂. It consisted of 80Å of Ag sputtered at a gas pressure of 5mTorr and at an RF of 50 W and a measured tooling factor of 218% and 2000Å of SiO₂ sputtered at a gas pressure of 5mTorr and at an RF of 300W and a tooling factor of 303%. Figure 4.10 shows a comparative study of the measured and the theoretical model.

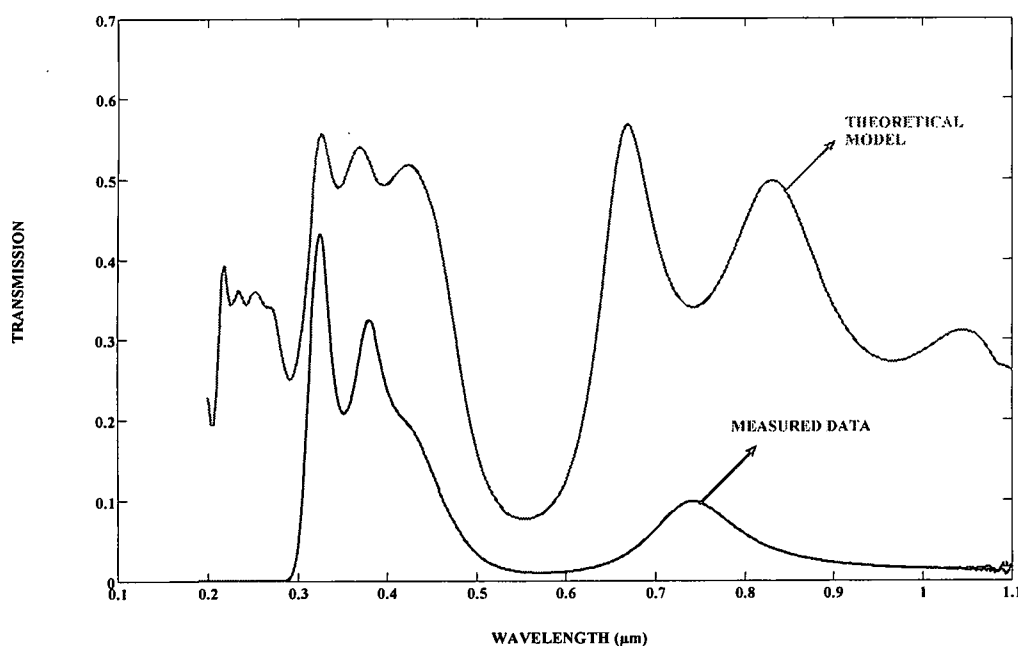


Figure 4.10 Fitting the measured data onto the theoretical model for stack-2A

There was no significant improvement in the result. The transmission was around 10% in the infrared region. There is some attenuation in the visible region. The new measured

tooling factor was 236% for Ag and 695% for SiO₂. Also the measured thickness of the entire stack was 9701Å for a deposited thickness of 8320Å as shown in the figure 4.11.

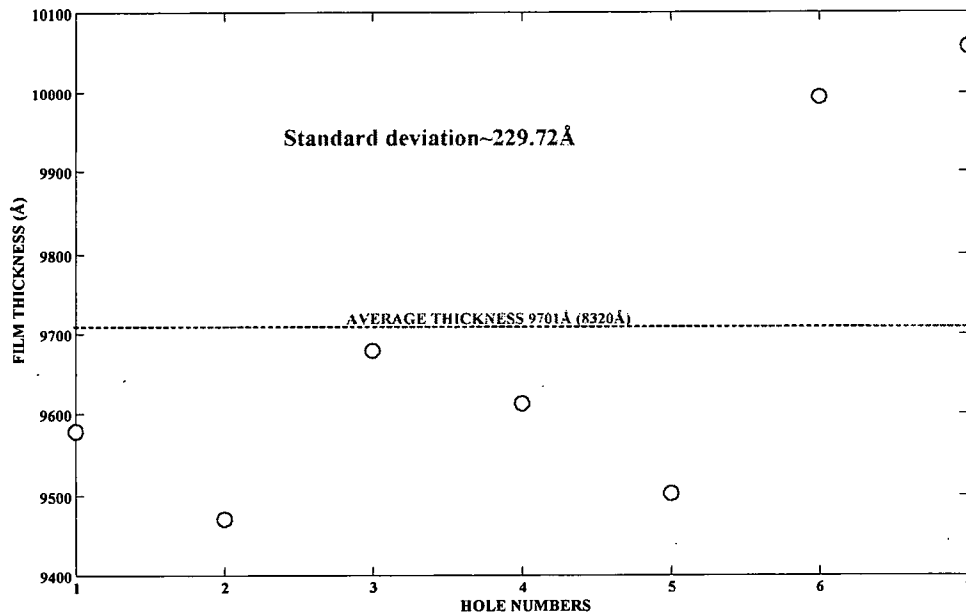


Figure 4.11 Thickness Measurement for MD stack-2A

MD (Metallo- Dielectric) stack-3

This stack was fabricated with 5 layers of SiO₂ (2000Å) sputtered at 300W and at a gas pressure of 5mTorr and 4 layers of Ag (50Å) sputtered at 50W at a gas pressure of 5mTorr. The main difference between the earlier stack and this was the change in the thickness of Ag layer and the tooling values for both the materials. Figure 4.12 shows a comparative study of the measured and the theoretical model for this stack.

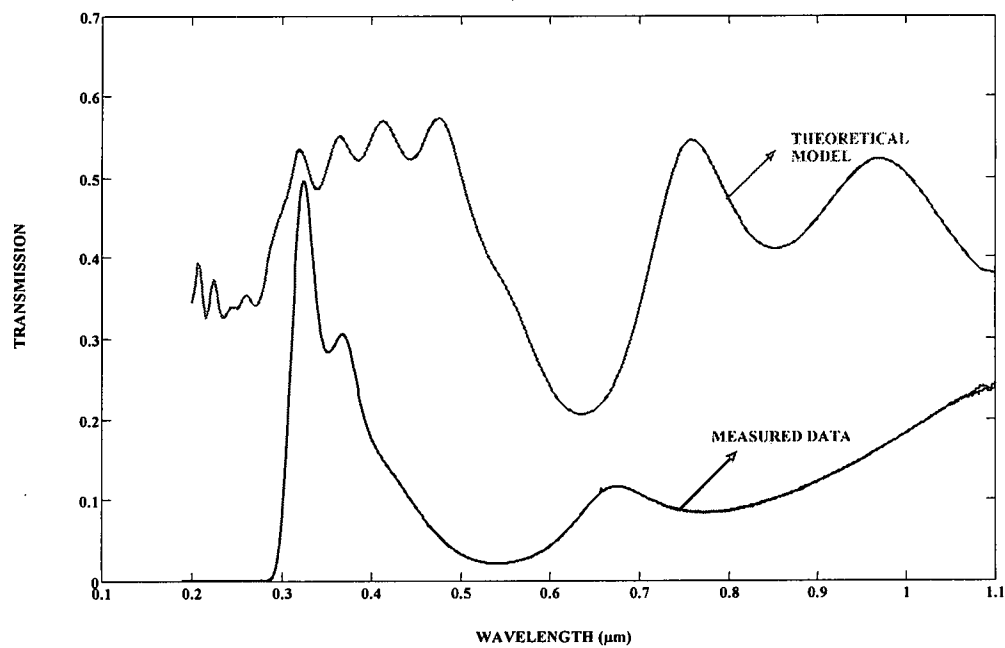


Figure 4.12 Fitting the measured data onto the theoretical model for stack-3

This design did not show a considerable change in the measured data either. The measured thickness of this stack was found to be 11,299Å for a deposited thickness of 10,200Å as shown in the figure 4.13.

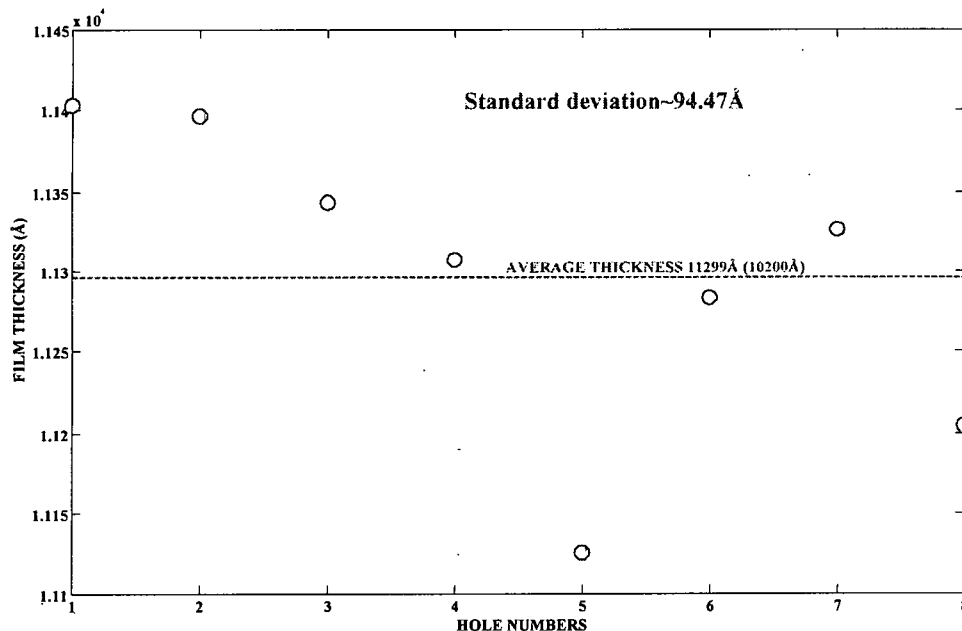


Figure 4.13 Thickness Measurement for MD stack-3

Another observation that was made was that the chamber had lots of yellow particulates in it and the SiO₂ shutter was all covered with these particulates. It was concluded that these yellow particulates were because of O₂ deficiency. It was not clear as to what actually caused these particulates. Since none of the designs could match the model, it was decided that the first stack be fabricated again except that we reduce the number of layers to 8.

MD (Metallo- Dielectric) stack-1A

This stack was fabricated with 4 pairs of SiO₂ (2300Å) sputtered at a gas pressure of 2mTorr and Ag (170Å) at a gas pressure of 2mTorr as well. Figure 4.14 shows a comparative study of the measured and the theoretical model for this stack.

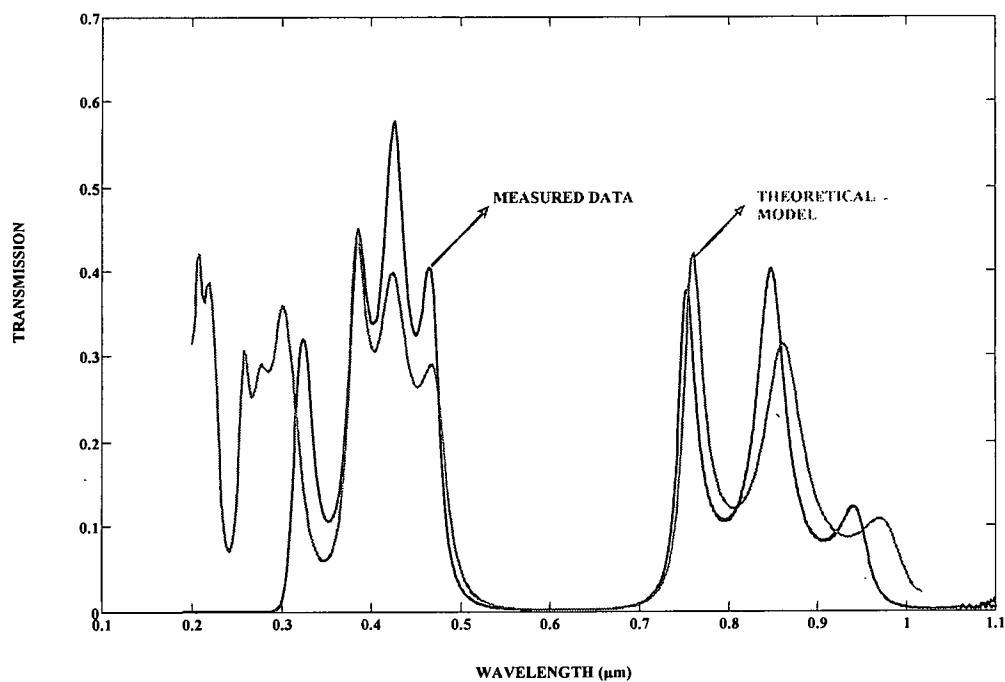


Figure 4.14 Fitting the measured data onto the theoretical model for stack-1A

It was observed that this stack had a transmission of around 60% in the visible region and also it matched well with the theoretical model. This was a better design in comparison to stack-1. Figure 4.15 shows the measured thickness of this stack. It was found to be 9327Å for a deposited thickness of 9880Å.

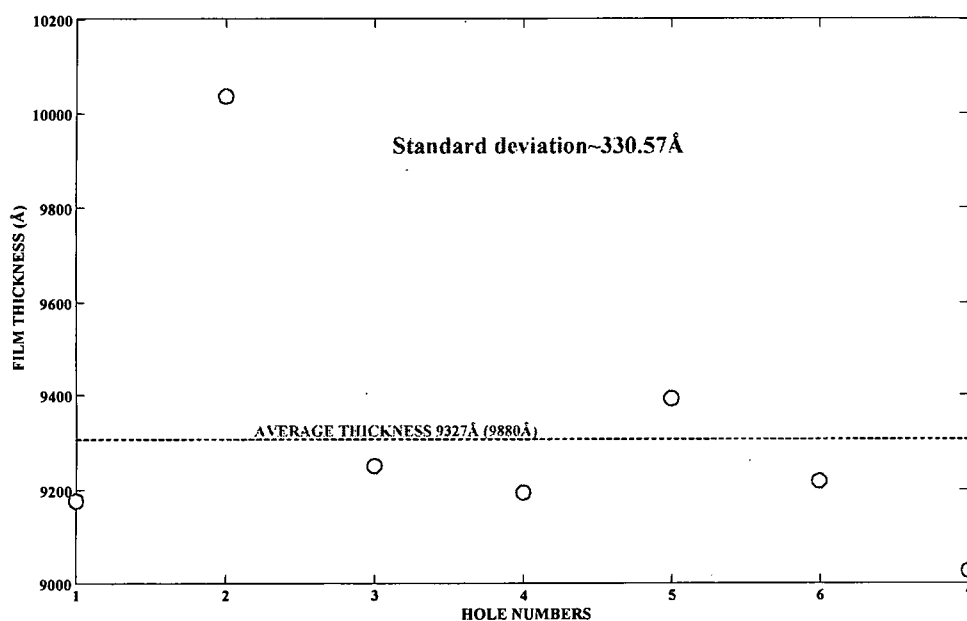


Figure 4.15 Thickness Measurement for MD stack-1A

It was observed that in comparison to the earlier stacks the thickness of this stack decreased in comparison to the deposited thickness. Also the chamber had yellow particulates which could be altering the thickness measurement and as a result altering the tooling value. One reason we thought for this variation in the different stacks could be because these yellow particulates were formed as a result of the O_2 that was liberated due to ionization. It is actually O_2 deficient SiO_2 . It is SiO_{2-x} i.e., SiO (Silicon Monoxide). Only some valence electrons were getting stripped off from the outer most shell of SiO_2 . As a result, the film that was being deposited was not pure SiO_2 . In order to avoid this SiO formation, 4%-6% of O_2 should also be bled into the chamber along with the process gas (Ar here) to validate for the stoichiometry. X-Ray Diffraction study of the sample deposited with SiO_2 will give the right amount of O_2 that needs to be released into the chamber along with Ar.

Another major factor affecting the thickness of these MD stacks is the thickness of Ag layers. In the case of 50Å and 80Å of Ag thicknesses, it is speculated that the films may not be uniform leading to incoherent interference. In the last design, 4 layers of 170Å were thick enough to produce a flat film by reducing the roughness and leading to coherent reflection and transmission. The problem could be verified by modifying the transfer matrix method to allow for both coherent and incoherent multiple reflections⁸ or performing the deposition with substrate heating to improve the uniformity of extremely thin layers.

Roughness Measurements for the Stacks

Similar to the roughness measurements described in chapter III, a roughness study was performed on all of the stacks fabricated for this study. Figure 4.16, 4.17 and 4.18 shows the results of the average roughness, RMS roughness and the peak to valley roughness for each of the stacks in comparison to the rest.

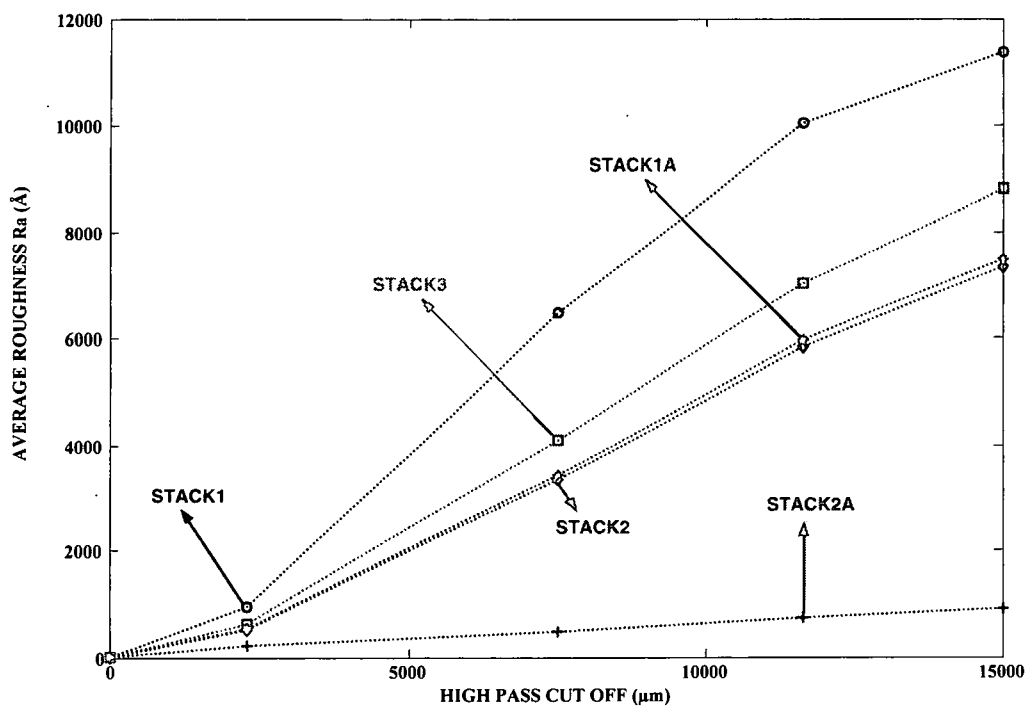


Figure 4.16 Average Roughness R_a Measurements

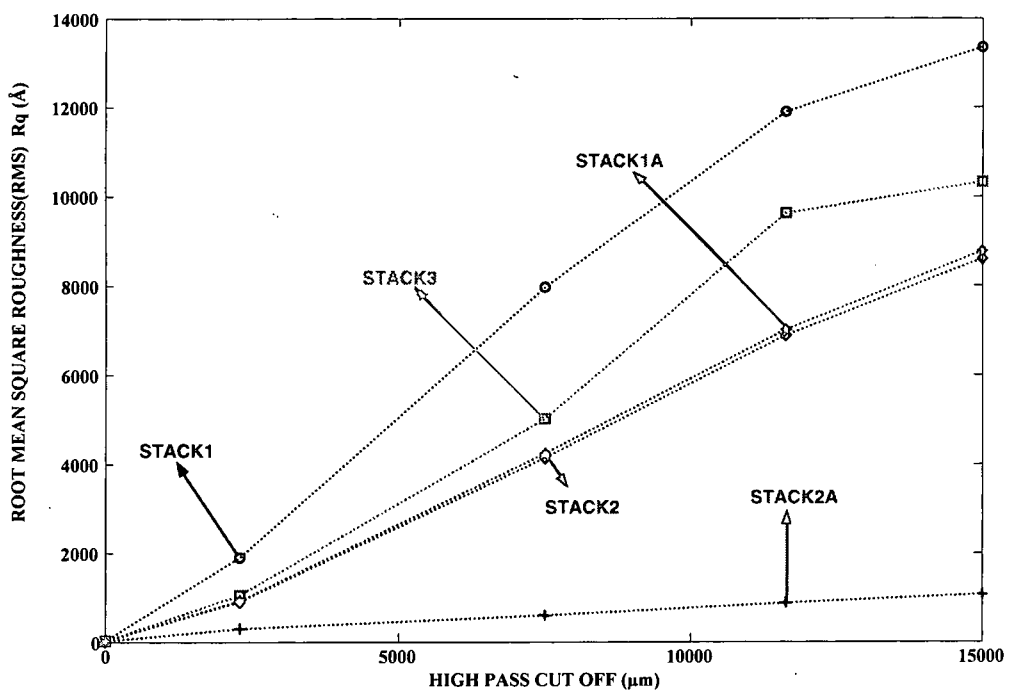


Figure 4.17 Root Mean Square (RMS) Roughness R_q Measurements

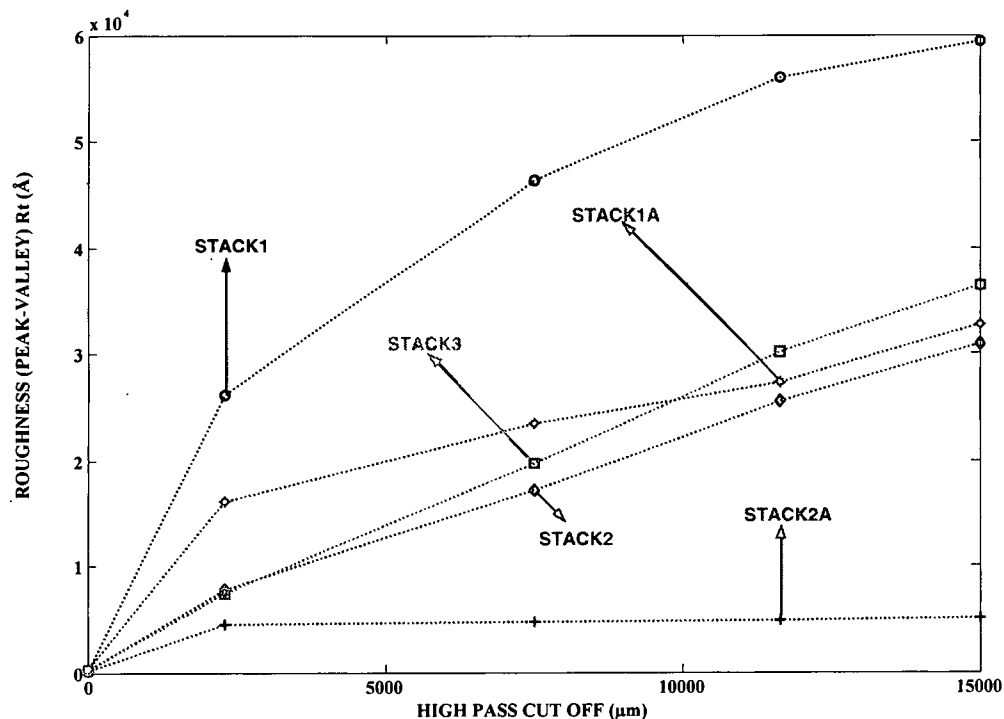


Figure 4.18 Roughness (Peak-Valley) R_t Roughness Measurements

It was observed that stack1 had the maximum roughness in comparison to the other stacks. Stack2A had the minimum roughness and the only one reason for this difference is the thickness of each of these stacks. Stack1 had an overall thickness of 15280Å (theoretical) and stack 2A had a measured thickness of 9701Å. The overall thickness for MD stack 2 was 8320Å (theoretical) and the measured thickness for stack 3 and 1A were 11,299Å and 9327Å respectively. It was difficult to conclude whether thickness played a major role in the roughness of the stacks from this study because each of these stacks was fabricated at a different process (Ar) gas pressure.

CHAPTER V

CONCLUSIONS

Conclusions

1. A multilayer stack made of a metal and a dielectric has been studied to increase the overall transmission in the visible region by altering the thickness of the metal layers and so this could be used as an optical filter to block some wavelengths of light and pass the required wavelengths.
2. Five different stacks were fabricated using 4 pairs of SiO_2 and Ag layers using RF magnetron sputtering by varying the thicknesses of the metal-dielectric layers.
3. MD Stack-1A was the one that gave a good fit to the model. The Transmission in the visible region was around 60%. The transmission at the band edge (pass band) was around 38%. There is reflection in the band gap from 500nm-700nm.
4. Thin film stress and roughness plays an important role in the performance of these stacks. In order to reduce the stress, a flat substrate has to be selected. The stress values were very high in this study because of the glass substrate which was already stressed prior to the film deposition.
5. The RF power at which the films are sputtered does not play a major role in the roughness of thin films as was seen in the study explained in chapter III.

6. As the gas pressure increases the rate increases and then remains a constant. The material has to be sputtered at this optimum rate. Also for different materials the tooling factor increases with increasing gas pressure as the flux distribution varies.

Summary of Contributions

The results of this study have contributed to the knowledge in the fabrication of MD stacks using RF magnetron sputtering. The performance of these stacks not just depends on the thickness of the metal and dielectric layers but also on the sputtering parameters. This study contributed to the fact that the deposition rate changes with gas pressure and hence the tooling factor for each material also changes. RF power was not a major contributor to the roughness of the thin films. There were two different stress measurements on Ag because the Ag film on the glass substrate induced different stresses on the substrate as the substrate itself was already bent. The chamber has to be very clean to fabricate these thin films. Also when depositing dielectric or optical materials, the life of a gold quartz monitor crystal is much shorter as much as 10% to 20% and this is due to the thermal and intrinsic stresses at the quartz-dielectric film interface.

Another major factor affecting the thickness of these MD stacks is the thickness of Ag layers. In the case of 50Å and 80Å of Ag thicknesses, it is speculated that the films may not be uniform leading to incoherent interference. In the last design, 4 layers of 170Å were thick enough to produce a flat film by reducing the roughness and leading to coherent reflection and transmission. The problem could be verified by modifying the transfer matrix method to allow for both coherent and incoherent multiple reflections or

performing the deposition with substrate heating to improve the uniformity of extremely thin layers.

Future Research

1. In the future a study of RF power with different film thicknesses at a constant process gas pressure could be done to verify if thicknesses were a major factor that contributed to film roughness. Also a 2-D scan for roughness could be done with varying RF powers instead of a 1-D scan.
2. Another way of obtaining really flat thin films is by controlling the substrate temperature. The present Denton vacuum sputtering system has no control over the substrate temperature but in the future this could be modified by may be using a thermocouple.
3. In the future the roughness measurements obtained using the Ambios profiler can be compared to that obtained using ellipsometry techniques and one can obtain a better method to measure thin film roughness.
4. After several depositions, yellow particulate formations were observed in the chamber which could be affecting the stack performance. In the future the system could be modified to include an O₂ bleed so that right amount of O₂ can be released into the chamber to compensate for the O₂ deficient, SiO₂ - x particles by studying the thin films deposited using X-Ray Diffraction.
5. Since SiO₂ and Ag, the two materials involved in this study has different sputtering parameters, in the future various other materials like Ge, ZnS, Si₃N₄, Si should be sputtered and their behavior should also be studied.

6. In the future the TMM program should be modified to include incoherent reflections coming from the various metal layers due to surface roughness.

REFERENCES

1. M.C. Larciprete, C.Sibilia, S.Paoloni, M. Bertolotti, F.Sarto, M.Scalora, "Accessing the optical limiting properties of metallo-dielectric photonic band gap structures" *Journal of Applied Physics*, Vol 93, No. 9, 2003.
2. M. Scalora, M.J. Bloemer, A.S. Pethel, J.P. Dowling, C.M. Bowden, A.S. Manka, "Transparent, metallo-dielectric, one-dimensional, photonic band-gap structures", *Journal of Applied Physics*, Vol 83, No. 5, 1998.
3. Anan Fang, Weiyi Zhang, Zhenlin Wang, An Hu and Naiben Ming, "Photonic band gaps of AB₃ and B₃ structures of metallodielectric spheres", *Journal of Physics: Condensed Matter* 13 (2001) 8489–8496.
4. Kenneth A. Epstein, David K. Misemer, and George D. Vernstrom, "Optical parameters of absorbing semiconductors from transmission and reflection", *Applied Optics*, Vol. 26, No.2, 1987.
5. David A.B. Miller, "Refractive Fabry-Perot bistability with linear absorption: theory of operation and cavity optimization", *IEEE Journal of Quantum Electronics*, Vol. QE-17, No.3, 1981.
6. M.Scalora, M.J. Bloemer, A.S. Pethel, J.P. Dowling, C.M. Bowden, and A.S. Manka, "Transparent, metallo-dielectric, one-dimensional, photonic band-gap structures", *Journal of Applied Physics*, Vol. 83, No.5, 1998.

7. Zoran Jaksic, Milan Maksimovic and Milija Sarajlic, "Silver-Silica transparent metal structures as band pass filters for the ultraviolet range", *Journal of Optics: Pure and Applied Optics*, 7(2005) 51-55.
8. Charalambos C. Katsidis and Dimitrios I. Siapkas, "General transfer-matrix method for optical multilayer systems with coherent, partially coherent, and incoherent interference", *Journal of Applied Optics*, Vol. 41, No.19, 2002.
9. B Mendez, F Dominguez-Adame and E Macia, "A transfer matrix method for the determination of one-dimensional band structures", *Journal of Physics, A: Math.Gen.*26(1993) 171-177.
10. J.F. Whitacre, Z.U. Rek, J.C. Bilello and S.M. Yalisove, "Surface roughness and in-plane texturing in sputtered thin films", *Journal of Applied Physics*, Vol.84, No.3, 1998.
11. Rabi Rabady and Ivan Avrutsky, "Reduced surface roughness of solid thin films prepared by alternating bias, radio-frequency magnetron sputtering", *Journal of Optical Society of America, B*, Vol.20, No.10, 2003
12. Stephen A. Campbell, "The Science and Engineering of Microelectronic Fabrication", Oxford University Press, Newyork, USA, 1996, p.281-332.
13. Kiyotaka Wasa and Shigeru Hayakawa, "Handbook of Sputter Deposition Technology, Principles, Technology and Applications", Noyes publications, New Jersey, USA, 1992, p.1-121.
14. Edward D. Palik, "Handbook of Optical Constants of Solids", Academic press, USA, 1998, p.759-760.

15. Kujotaka Wasa, Makoto Kitobataka and Hideaki Adachi, "Thin Film Materials Technology, Sputtering of Compound Materials", William Andrew publications, NY, USA, 2004, p.17-173.
16. Milton Ohring, "The materials Science of Thin Films", Academic Press, USA, 2002, p.277-349.
17. The various sputtering techniques were taken from the Physics of Thin films course offered at UCCS.
<http://www.uccs.edu/~tchrste/courses/PHYS549/549lectures/sputtertech.html>
18. Andrew M.Sarangan, "Nanophotonics", Class notes, winter semester, 2005.
19. Information on Bonding of Sputter Targets from Cougar Labs Inc.,
<http://www.cougarlabs.com/bond1.html>
20. Andrew M. Sarangan, "Integrated Optics Handbook", EOP -604, 2005.
21. Agilent 8453 UV-visible Spectroscopy System, Handbook,2002-2003.
<http://www.chem.agilent.com/scripts/pds.asp?lPage=298>
22. XTM/2 Inficon Thin Film Deposition Monitor, Operating Manual, 2001.
23. Ambios XP Series Stylus profiler Users manual, 2005
24. Denton Vacuum Explorer 14 Coating System: Turbo Pump, Sputter deposition system, Operating Manual, 2004.
25. Pier 10, "Progress in Electromagnetics Research and Methods for Modeling and Simulation of Guided-Wave Optoelectronic Devices: partI: Modes and Couplings", EMW publishing, Cambridge, MA, USA, 1995, p.271-286
26. Spin Coating information from <http://www.mse.arizona.edu/faculty/birnie/Coatings/> and <http://www.polymerprocessing.com/operations/spcoat/>

VITA

June 18, 1978	Born-Secunderabad, Andhra Pradesh (AP), India
1998	B.S., St.Francis College, Hyderabad, AP, India
1999	Bachelor's in Education, St.Ann's College, AP, India
2002	M.S., Applied Electronics, Osmania University, India
2003	Lecturer in Physics, Shadhan Institute of Post Graduate Studies, AP, India
2004-2005	Graduate Teaching Assistant, Department of Physics University of Dayton, Dayton, Ohio
2005	Graduate Research Assistant, Nanofabrication clean room facility, University of Dayton, Dayton, Ohio
2005	M.S., University of Dayton, Dayton, Ohio

CONFERENCE APPERANCES

Metallo-dielectric Photonic Band Gap Materials fabricated using Thin Film Technology, Liquid Crystals in Optics and Photonics in Conjunction with fall 2005 meeting of the Great Lakes SPIE regional Chapter, Kent State University, Kent, Ohio.

FIELDS OF STUDY

Major field: Optoelectronic device fabrication

R002592442

HECKMAN

BINDERY, INC

T 024891 E 17 00



1/19/2006

Metallo-dielectric Photonic Band Gap Structures Fabricated using RF Magnetron Sputtering Technology, Professor Andrew M. Sarangan